Department of Human and Engineered Environmental Studies
Graduate School of Frontier Sciences
The University of Tokyo

2019

Master's Thesis

高倍率集光型太陽電池冷却用相変化冷却器に関する研究 (Study on two phase cooling unit applied for high concentration solar cell)

Submitted February 6th, 2020

Adviser: Professor Dang Chaobin (seal)

Student ID Number 47123456

Zhang Bohan

Contents

Chapter 1 Introduction

1.1. Research background

1.1.1 Photovoltaic system

Energy is one of the vital factors for any country development. Till date the coal as one of the major sources of electricity production has the share of electricity by 42% and it will still be the main source of electricity in many countries in the next few decades [1]. But the problems of worldwide energy shortage and environment pollution are becoming more serious, so renewable energy has been encouraged by many countries due to the advantages of being sustainable and not contributing to the world's CO2 greenhouse gas emissions [2]. Solar energy as an abundant and large potential renewable energy source in the world has no pollution [3], so it has been widely used. Such a system generates electricity by converting the Sun's energy directly into electricity. According to 2015's data, solar photovoltaics (PV) contribute about 227 GW, and concentrating solar power (CSP) technologies contribute about 4.8 GW in electricity generation capacity [4].

A photovoltaic (PV) system is a system composed of one or more solar panels combined with an inverter and other electrical and mechanical hardware that use energy from the Sun to generate electricity. Fig.1.1 is a sample of a classical PV system for civil use. PV systems can vary greatly in size from small rooftop or portable systems to massive utility-scale generation plants.

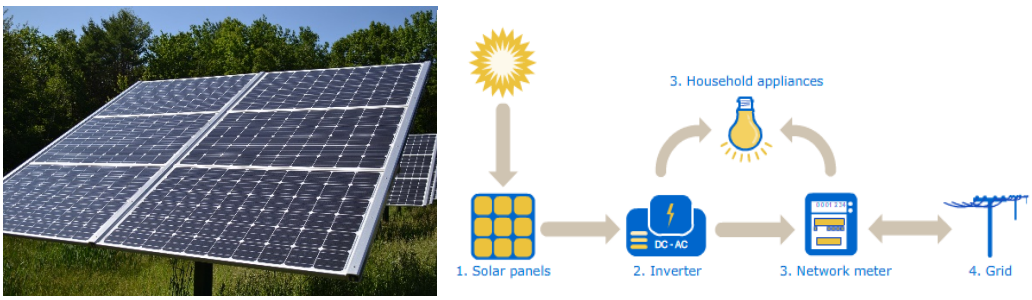

Fig.1.1: Residential grid-tied solar PV system

1.1.2 Solar thermal energy

A very common example to utilize solar thermal energy is the solar water heating (SWH),

which is widely used for residential and some industrial applications. Solar water heating is the conversion of sunlight into heat for water heating using a solar thermal collector. A sun-facing collector heats a working fluid that passes into a storage system for later use. SWH is an active and reliable way to converse solar energy to thermal energy. They are heated directly or via light-concentrating mirrors. They operate independently or as hybrids with electric or gas heaters.[5] In large-scale installations, mirrors may concentrate sunlight into a smaller collector.

However, with the desire to achieve solar energy more efficiently, parabolic trough is invented. Parabolic trough power plants (as seen in fig.1.2) use a curved, mirrored trough which reflects the direct solar radiation onto a glass tube containing a fluid running the length of the trough, positioned at the focal point of the reflectors. The receiver may be enclosed in a glass vacuum chamber. The vacuum significantly reduces convective heat loss. Heat transfer fluid passes through the receiver and becomes very hot. And the fluid containing the heat could be saved for civil use or other thermal applications.

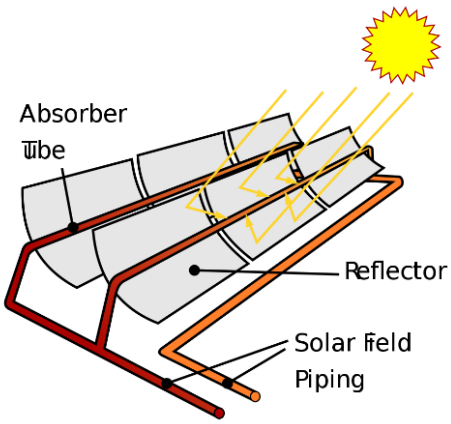

Fig.1.2: Sketch of a parabolic trough

1.1.3 High-concentration-photovoltaic-thermal system

Harvesting solar energy is a promising technology for renewable power generation with the potential to meet a significant proportion of the world's energy needs.

There are many alternatives available to directly harness the sun's energy. Both Photovoltaic and SWH are good methods to harness solar energy, but if we want to improve energy conversion efficiency more, high concentration photovoltaic thermal system (HCPVT), as seen in fig.1.3, would be the answer, which is a system that solar collectors designed to generate

thermal energy and photovoltaic cells generating electricity simultaneously.

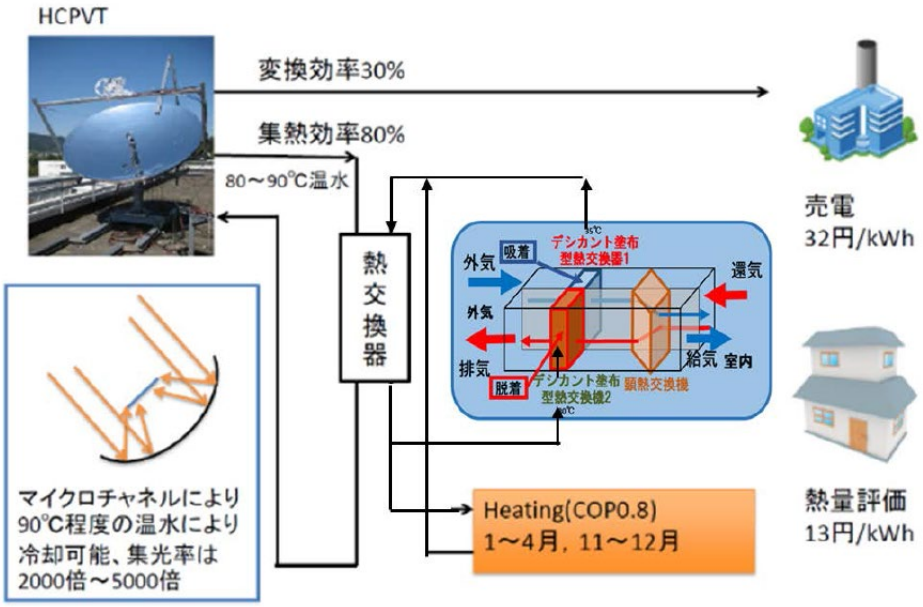

Fig.1.3: Concept of high concentration photovoltaic thermal system

The photovoltaic/thermal (PV/T) system is a hybrid system which produces both electricity and heat to increase the overall efficiency. The first investigation on PV/T system was presented by Wolf [6]. A significant amount of experimental and theoretical studies on PV/T collectors/systems have been conducted [7]. One of the disadvantages of PV/T systems is the high cost of photovoltaic because of the large demand for solar cells. Concentrator photovoltaic (CPV) system can reduce the area of solar cells by concentrating solar radiation onto solar cells. If the cost of tracking assembly and concentrator is less than the cost of the saved solar cells, it will be an effective way to reduce the total cost of the system [8]. The efficiency of multi-junction solar cells is reported to be higher than 40% [9], thus it shows great potential when applying the multi-junction solar cells in CPV systems. Some solar cells, especially some multi-junction solar cells, can work at high temperature up to 150°C while maintaining reasonable photovoltaic efficiency as reported in [10]. Concentrator increases the radiation intensity and heat flux on solar cell. Collecting the heat from a CPV system leads to a CPV/T system, providing both electricity and heat. A plenty of researches and developments have been conducted on CPV/T systems about concentrator designing, system optimization and performance evaluation. According to the concentrator type, CPV/T systems can be classified as compound parabolic concentrator type (CPC) [11], parabolic trough type [12], dish type [13],

linear Fresnel type [14] and point-focus Fresnel type [15].

In this article, a parabolic dish concentrator (fig.1.4) is used to collect solar energy. The diameter of parabolic dish is 2m and focal length is 1.2m. The surface is consisting of huge aluminum reflective films that have a high reflectivity of 90%.

In order to utilize solar energy more efficiently, a tracking system is installed in concentrator. We apply a GPS/Photosensitive sensor tracker on the top of the concentrator (fig.1.5). Four photoresistors are set in each direction: east, west, north and south. When the sunlight shining into tracker, according to parallelism of light photoresistors can give an electrical signal to adjust concentrator to face the sun.

When a cloudy day, there is almost no sunshine could be received by photosensitive senor. The sun's position can be calculated by the time and location of concentrator by global position system (GPS).

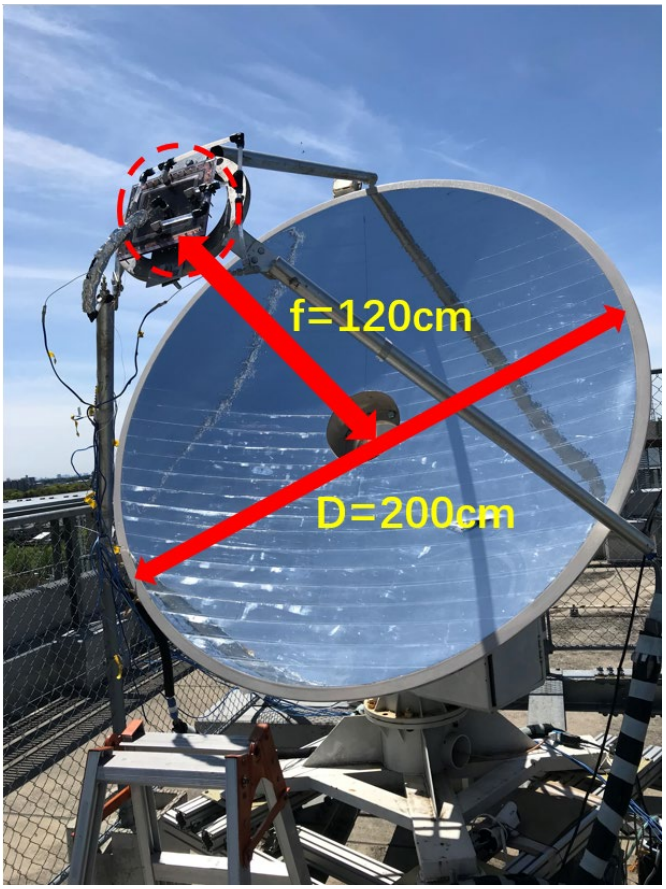

Fig.1.4: Photo of parabolic concentrator

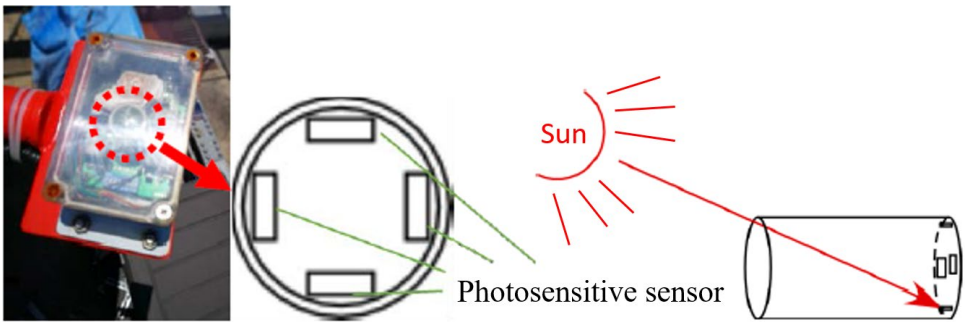

Fig.1.5: GPS/Photosensitive sensor tracker

1.1.4 Solar radiation

Solar radiation is radiant energy emitted by the sun from a nuclear fusion reaction that creates electromagnetic energy. On the other hand, solar radiation has a great effect on the thermal environment, lighting environment, and comfort including psychological aspects, as well as energy consumption for cooling, heating and lighting.

Solar radiant energy reaches the Earth's atmosphere about 1.37 kW/m2 which is called extraterrestrial radiation. Some of these are reflected, absorbed, and scattered before they enter the atmosphere and reach the surface. As a result, on the surface of the earth, as shown in Fig.1.6, the solar radiation is combined with direct solar radiation and diffuse solar radiation. (global solar radiation = direct solar radiation + diffuse solar radiation).

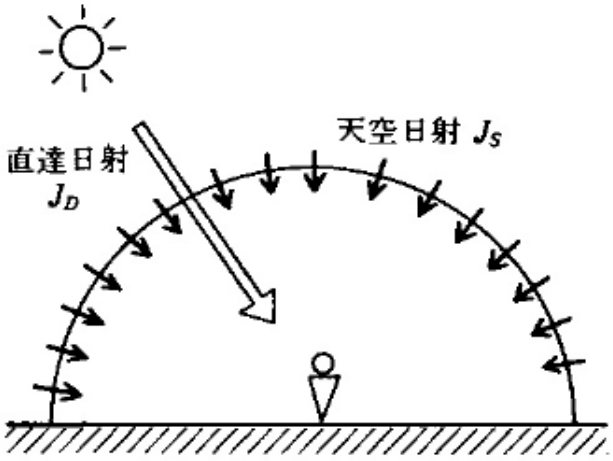

Fig.1.6: The composition of solar radiation

For conventional photovoltaic system, such as solar panels and solar water heating, they are usually fixed on the ground or on the rooftops. In that case, weather direct solar radiation or diffuse solar radiation all have contribution to energy conversion. However, parabolic dish

concentrator uses a solar tracker to follow the sun across the sky. As show in fig.1.7, only the direct solar radiation could be reflected by parabolic dish, that is to say direct solar radiation is the source of energy.

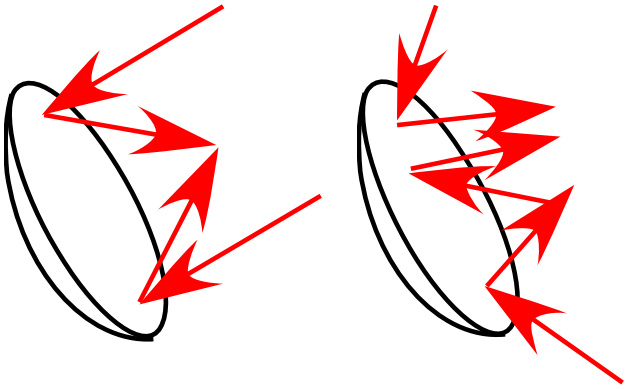

(a) Direct solar radiation (b) diffuse solar radiation

Fig.1.7: Radiation and parabolic dish concentrator

1.1.5 Concentration ratio

The solar concentration ratio is an important concept for a focusing solar collector. In order to achieve higher energy flux density, it is necessary to concentrate energy to one spot.

The definition of a concentration ratio of solar concentration is the ratio of solar radiation entering the collector to solar radiation received by the receiver, as Eq.1-1. It represents the system's ability to concentrate solar energy.

$$C_{geom} = \frac{A_{con}}{A_{spot}} \qquad (1-1)$$

The geometry concentration ratio is a parameter that does not change once the system is manufactured, it is convenient for application in practical engineering. However, in fact the concentration ratio equation should be revised with concentrator reflectance.

$$C = \alpha \cdot C_{geom} \qquad (1-2)$$

Where α is concentrator reflectance which is related to property of surface coating.

According to the parameter of parabolic dish, geometry concentration ratio can be calculated as $1061xsuns$ (1061 times of solar radiation).

For example, commonly, in a sunny day the direct solar radiation is about 800 W/m2, so the heat flux concentrated by parabolic dish concentrator will be 800×1061W/m2.

1.2. Cooling methods for concentration cell

1.2.1 Single-phase convective heat transfer

Single-phase cooling is a cooling method that uses a liquid refrigerant to exchange heat without phase change. Compared to air cooling, it has the advantage of higher heat transfer coefficient and silent. Since no phase change occurs, stable cooling is possible. However, since the single-phase flow is cooled by sensible heat, the temperature of the fluid rises along the flow direction, and a great temperature difference is generated on the cooling surface. In addition, the single-phase cooling requires the pump to drive the refrigerant, and has a disadvantage that the driving power is larger than the two-phase cooling.

1.2.2 Two-phase flow boiling heat transfer in micro-channel

Microchannel heat exchangers have the potential of achieving very high heat transfer rates compared to conventional heat exchangers due to the very high surface area to volume ratio. For example, Kang et al. [16] tested the performance of a cross flow microchannel heat exchanger using de-ionized water. The core volume of this heat exchanger was 0.918 cm^3 and consisted of 26 stacked layers of silicon substrate with 125 channels etched on top of each layer resulting in a total surface area to volume ratio of 15,294 m^2/m^3. They reported that the heat transfer rate between the hot and cold fluid streams reached 5 kW at 4.5 l/min liquid flow rate, 2.47 bar pressure drop and 30 K mean temperature difference. In other words, this micro heat exchanger achieved a volumetric heat transfer rate of 5.44 GW/m^3 at about 24W pumping power. This value is huge compared to existing compact heat exchangers. For instance, using the specifications published by a typical heat exchanger manufacturer, one can see that a compact heat exchanger of 12 kW has overall dimensions of 1630 cm^3, weights approximately 3 kg, has a surface area to volume ratio of 650 m^2/m^3 and a volumetric heat transfer rate of approximately only 14 MW/m^3. This example demonstrates that the surface area to volume ratio and the heat transfer rate per unit volume of microchannel heat exchangers are significantly higher than that of typical compact heat exchangers.

Moreover, microchannel heat exchanger has another advantage in HCPVT system. When

using water as a working fluid, the outlet temperature of microchannel heat exchanger is over 100℃. This high exergy energy could be applied on other thermal applications such as, adsorption chiller, desalination and etc. By two-phase flow cooling the usefulness of the thermal energy extracted from the heat exchanger is much higher than space cooling or single-phase flow cooling, so two-phase flow cooling can greatly improve overall system performance.

Based on that, more research was conducted in the last two decades towards investigating flow boiling in microchannel heat exchangers with the objective of cooling high heat flux systems, the parabolic dish concentrator is a great example of them. To cool down the solar cell and recovery of low exergy energy, flow boiling heat transfer is the best answer.

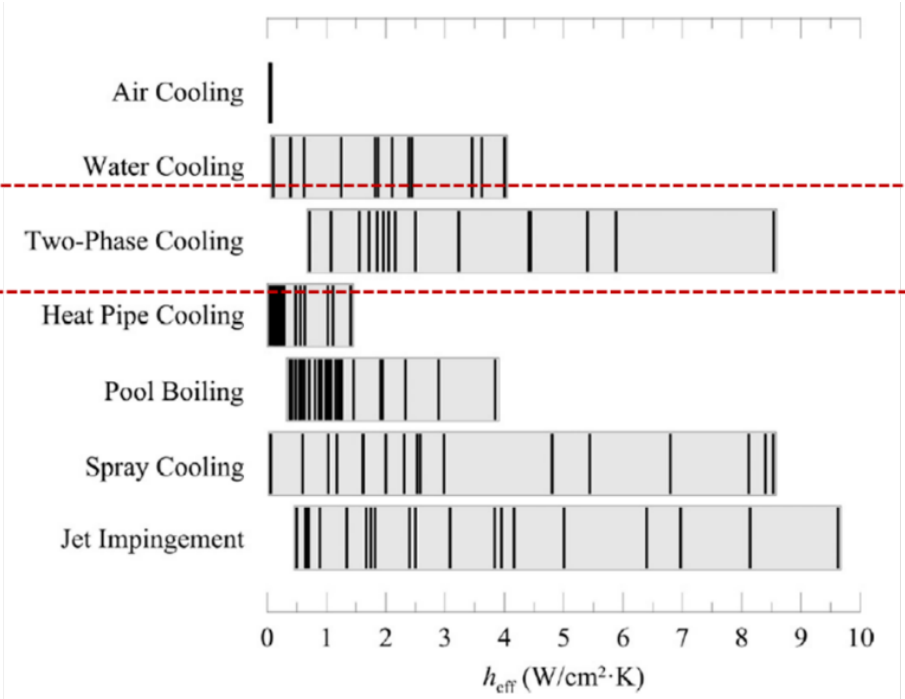

Fig.1.8: Comparison of effective heat transfer coefficient for different cooling technologies

The significant advantages of using flow boiling in these systems can be summarized as follows:

(1) Flow boiling can achieve small variations in the surface temperature (almost uniform at values slightly above the saturation temperature). This can improve the durability of the electronic equipment significantly due to the reduction of the thermo-mechanical stresses inside the chip. In this article, temperature of solar cell needs to be strictly controlled below 150 degrees or the cell would be burned. So, it is very approbative to utilize flow boiling heat transfer in the HCPVT system.

(2) The capability of achieving very high heat transfer rates at small liquid flowrates compared to single phase cooling. This means that a small liquid pump is required resulting in a very compact cooling system.

(3) Two-phase flow cooling has a great capability of heat transfer performance, which means the temperature difference of flow and wall will be very small and it is possible to create a safe working condition for triple-junction solar cell.

(4) Because of the high exergy flow generated by micro-channel heat exchanger. Two-phase flow heat transfer can elevate the overall system energy conversion efficient.

When the nucleate boiling becomes the dominant heat transfer mechanism in micro-channels, another two advantages may be added.

The first one is the increase of the heat transfer coefficient with increasing heat flux in nucleate boiling. This will result in very small variations in the chip temperature when the heat dissipation rate varies (increase/decrease). For example, for flow boiling of R-134a in a 1 mm diameter tube when the heat flux was increased from 13 kW/m^2 to 25 kW/m^2, the heat transfer coefficient increased from 6000 $W/m\ ^2K$ to 8000 $W/m\ ^2K$, see Mahmoud et al. [17]. Based on these values at 8 bar system pressure ($Tsat = 31.3$℃), the surface temperature increases only by 3% for this 12 kW/m^2 increase in heat flux. In contrast, if single phase liquid cooling was used, the surface temperature increases by about 60%. The significant variations in chip temperature in single phase flow when the heat dissipation rate varies may affect the lifetime of the electronic equipment. The second advantage of nucleate boiling is the independence of the heat transfer coefficient on mass flux. This makes it possible to use a fixed speed pump, i.e. no need for a speed controller, which will result in a simpler and more reliable cooling system at a reduced cost.

The design of such two-phase flow micro-channel heat sink involves an understanding of flow regimes, pressure drop, flow instabilities and heat transfer coefficient.

1.3. Flow regime

Single-phase flow is classified into laminar flow and turbulent flow, and their heat transfer characteristics are different. The flow regime of two-phase flow is complicated, and shows different flow characteristics and heat transfer coefficient on each flow regime. In that way, the

research of the flow regime is necessary.

Although there are still arguments on the classification of the flow patterns, most researchers agreed to categorize their observations into four main flow patterns: stratified flow, intermittent flow, annular flow and bubble flow. Each main class could be subdivided into subclasses.

Taitel [18] and Barnea [19] defined five typical flow patterns in their vertical upward flow pattern map, i.e. dispersed bubble, bubbly, slug, churn and annular.

These are as follows (Fig.1.9):

Dispersed bubble: numerous small bubbles float in a continuous liquid phase.

Bubbly: bubble size is comparable to but not as large as the tube diameter.

Slug: bubbles develop into bullet shape due to the tube wall restriction. Sometimes the bullet bubbles are followed by a stream of small bubbles creating a trail.

Churn: bullet bubbles start to distort and small bubbles in liquid slug coalesce into gas clump with increase of gas velocity. It is a highly oscillatory flow with chaotic interface.

Annular: gas phase becomes a continuous flow in the core of the tube.

Mist: liquid film is blown away from tube wall and numerous liquid droplets float in high-speed

vapor flow.

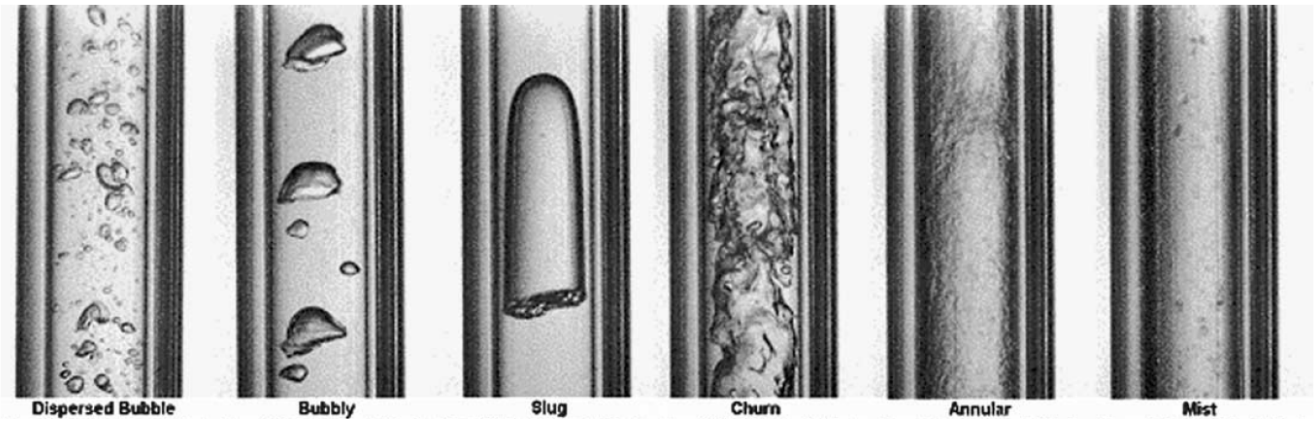

Fig.1.9: Flow patterns observed in 4.26 mm internal diameter tube at 10 bar

Actually, flow pattern is closely related to local heat transfer coefficient because vapor quality in each flow pattern is different from others and vapor quality has influence on the formation of boundary layer. So, it is essential to figure out the relationship between flow

pattern (vapor quality) and heat transfer coefficient.

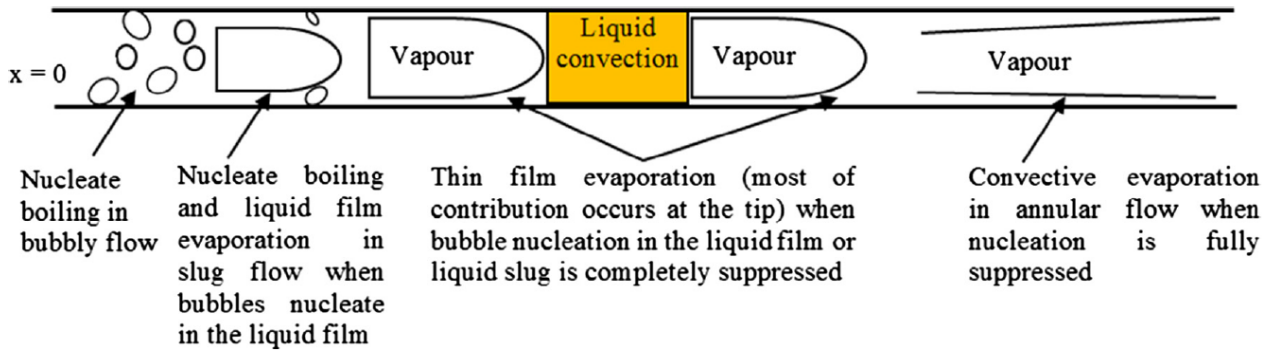

Fig. 1.10. Schematic drawing for the different mechanisms in flow boiling in small to micro diameter channels.

Thome [20] compared the experimental data of recent microchannels with the heat transfer model and summarized the mechanism of flow boiling heat transfer in the microchannel in terms of the two-phase flow pattern and the flow boiling heat transfer mechanism. In the low vapor quality region of the microchannel, nucleate boiling is the main heat transfer mechanism, and in the high vapor quality region, the nucleate boiling is suppressed and the liquid film evaporation is the main heat transfer mechanism. Saturation pressure, heat flux, mass velocity and quality have a great influence on heat transfer. In particular, in the low mass velocity region of less than 100 kg/m^2s, inertia force, surface tension, and shear force in the pipe is different from that in the high mass velocity region, so the flow pattern also differs. In a word, flow regime has a close relationship with local heat transfer coefficient in micro-channels, and from the flow regime, it is possible to judge whether there is a stable boiling heat transfer occurred in micro-channel or not.

1.4. Two-phase flow pressure drop

Two-phase flow pressure drop has been one of the most formidable issues since the 1940's. To predict two-phase flow pressure drop is very necessary. In a two-phase flow system, the pressure drop determines required pump drive power, so if the pressure drop can be predicted correctly, it will lead to an improvement of effective use of energy and a simplified design. The pressure loss of a two-phase flow consists of the gravity term, friction pressure drop and acceleration pressure drop. Usually in a microchannel, the static pressure drop is extremely small. Friction is affected by the shear force at the gas-liquid interface and by the turbulence

caused by the motion of the gas phase or bubbles. When the mass flow is low, these effects become significant. Acceleration drop is based on the momentum difference between the inlet and the outlet of the pipe, the proportion of acceleration pressure drop in the pipe is generally small. However, when under a high heat flux working condition, it is on the same order as friction pressure drop. [21]

Lockhart and Martinelli separated flow model [22] is able to calculate pressure drop when under a high heat flux and it is the most common way to calculate two-phase flow pressure drop based on a two-phase multiplier for the liquid-phase, or the vapor-phase, respectively.

The two-phase pressure drops for flows inside tubes are the sum of three contributions: the static pressure drop ΔP_{static}, the acceleration pressure drop ΔP_{acc} and the frictional pressure drop ΔP_f as:

$$\Delta P_{total} = \Delta P_{static} + \Delta P_{acc} + \Delta P_f \qquad (1-3)$$

The static pressure drop is given by:

$$\Delta P_{static} = \rho_{tp} g H \sin\theta \qquad (1-4)$$

Where θ is the angle of inclination, average density of two-phase flow ρ_{tp} is obtained from:

$$\rho_{tp} = \rho_l(1-\alpha) + \rho_g \alpha \qquad (1-5)$$

The void fraction α is given by:

$$\alpha = \left[1 + \left(\frac{1-x}{x}\right)\left(\frac{\rho_v}{\rho_L}\right)^{\frac{2}{3}}\right]^{-1} \qquad (1-6)$$

Where x is vapor quality.

The acceleration pressure drop reflects the change in kinetic energy of the flow and is given by:

$$\Delta P_{\mathrm{acc}} = \frac{G^2}{\rho_L}\left[\frac{x_{\mathrm{out}}^2}{\alpha_{\mathrm{out}}}\left(\frac{\rho_{\mathrm{L}}}{\rho_{\mathrm{v}}}\right) + \frac{(1-x_{\mathrm{out}})^2}{1-\alpha_{\mathrm{out}}} - 1\right] \qquad (1-7)$$

The friction pressure drop is given by:

$$\Delta P_{\mathrm{f}} = \frac{2G^2 L_{\mathrm{tp}}}{d_{\mathrm{h}} x_{\mathrm{out}}} \int_{x_{\mathrm{in}}}^{x_{\mathrm{out}}} \frac{f_{\mathrm{r}}(1-x)\phi_{\mathrm{L}}^2}{\rho_l} \mathrm{d}x \qquad (1-8)$$

Friction factor f_r is defined as:

$$f_r = \begin{cases} 16Re^{-1} & ,for\ \ Re < 2000 \\ 0.079Re^{-0.25} & ,for\ \ 2000 \le Re < 20000 \\ 0.046Re^{-0.2} & ,for\ \ 20000 \le Re \end{cases} \qquad (1-9)$$

Φ_L^2 is defined as:

$$\Phi_L^2 = 1 + \frac{C}{X} + \frac{1}{X^2} \qquad (1-10)$$

where X is the Martinelli parameter defined as:

$$X^2 = \left[\frac{\left(\frac{dP}{dz}\right)_L}{\left(\frac{dP}{dz}\right)_v}\right] \qquad (1-11)$$

Where d_{h} is hydraulic diameter, G is mass velocity.

The value of C in Eq. (1-10) depends on the regimes of the liquid and vapor. The appropriate values to use are listed in Table 1.1. The correlation of Lockhart and Martinelli is applicable to the vapor quality range of $0 < x \leq 1$.

Table.1.1: Values of C

Liquid	*Gas*	*C*
Turbulence	Turbulence	20
Laminar	Turbulence	12
Turbulence	Laminar	10
Laminar	Laminar	5

1.5. Two-phase flow instability

Flow boiling instability is a critical issue that should be taken into consideration during the design of micro evaporators. It might have a dramatic effect on the overall system performance. Once the flow becomes unstable, all system parameters such as mass flow rate, pressure and temperature oscillate with large amplitudes. These amplitudes can be as high as 36 K for wall temperature, as found by Wang et al. [23], and 992.4 kg/m2 s and 60 kPa for mass flux and pressure drop, respectively, as found by Fu et al. [24]. Thus, the local time averaged heat transfer coefficient may be strongly influenced by these fluctuations. Understanding the reasons for instabilities may help find solution to this issue. The possible reasons for flow instability can be summarized as follows:

1. Rapid bubble growth and expansion in the upstream and downstream sides of the channel. This explanation was reported by [25]. At this condition, it was observed by all the above that the bubble remains stationary for a very short time period with small axial oscillations or slides slowly forward. Accordingly, evaporation of the thin liquid layer underneath the bubble during this period results in the formation of a dry patch, which is responsible for the instantaneous

jump in the wall temperature. When the bubble departs and moves away from the nucleation site, fresh liquid wets the surface and the wall temperature drops again.

2. Size of outlet section − single channel. This reason was proposed by Qi et al. [26] who investigated flow boiling of liquid nitrogen in four cold drawn stainless-steel tubes having diameters of 0.531, 0.834, 1.042 and 1.931 mm. The test sections were connected between two plenums with diameters larger than the test section diameter, i.e. inlet and outlet restrictions. They attributed the instability observed in their experiment to the effect of the outlet restriction (outlet plenum) and they explained it as follows: after boiling incipience, small bubbles move downstream and enter the outlet plenum, where their velocity decreases due to the sudden area enlargement. As a result, more bubbles accumulate inside the plenum, resulting in the formation of a large vapor patch, which can cause a temporary blockage. This blockage leads to a sharp decrease in mass flux, which in turn results in an increase in the wall temperature and vapor quality. The sudden increase in vapor quality, due to the reduction in mass flow rate, results in a sudden peak in pressure drop. Once the vapor patch passes through the outlet restriction, fresh liquid enters the tube and the mass flux increases again, improving the heat transfer process and reducing wall temperature.

3. Nucleation near the channel inlet. Kandlikar [27] discussed nucleation and instability in microchannels and reported that the location of boiling incipience affected flow reversal, and thus the oscillation in the measured parameters such as pressure and temperature. When nucleation occurred near the channel exit, the flow resistance in the back flow direction increased and consequently no flow reversal occurred (stable flow). On the contrary, when nucleation occurred near the channel inlet, the flow resistance in the backflow direction decreased and thus flow reversal occurred (unstable flow).

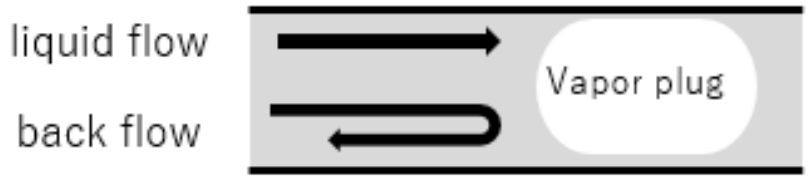

Fig.1.11: Reverse flow in micro-channel

An example of flow reversal in microchannels was given by Fayyadh et al. [28]. They

investigated flow boiling of R134a in a copper, multi-microchannel evaporator having a 0.3 mm channel width, a 0.7 mm channel height, a 0.2 mm fin thickness and a 20 mm channel length. The channels were cut on the top of a copper block, while the manifold and plenum were cut in the polycarbonate housing block. The fluid entered the channels through a deep plenum and a manifold with a convergent cross-sectional area and the same depth as the channel. It left the channel through a manifold with a divergent cross section area into a deep outlet plenum. The mass flux ranged from 50 to 300 kg/m2 s. It was found that, for G = 50 kg/m2 s, flow reversal occurred at boiling incipience and continued for all heat fluxes. Fig. 11 shows the sequence of pictures for flow reversal occurring at boiling incipience for P = 6.5 bar and G = 50 kg/m2 s. It is obvious from the pictures that the vapor patch stays for about 210 ms in the inlet manifold, with back and forth motion, before its rupture into segmented bubbles that moved downstream. As the mass flux increased, the heat flux at which flow reversal occurred increased. Very mild flow reversal was observed in the inlet manifold at a base heat flux of 149 kW/m2 for G = 300 kg/m2 s, where the vapor patch stayed only for about 10 ms in the inlet manifold.

1.6. Calculation of heat transfer coefficient of micro-channel

With advance of state-of-the-art micro-scale technologies and demands for more high cooling efficiency in such practical applications as the cooling of diverters of fusion reactors, high performance electronic chips, compact heat exchangers and other heat transfer devices, research work on heat transfer coefficient of micro-channels has never stopped.

Some common correlations for predicting saturated flow boiling heat transfer coefficients in conventional channels will be reviewed briefly. As well known, flow boiling heat transfer is governed mainly by two important mechanisms: nucleate boiling and forced convection. So far it is not well understood yet how these two mechanisms are superimposed in the flow boiling field. Three kinds of models exist in the literature, one by Chen [29], using addition of two components corresponding to the two mechanisms with a suppression factor and a Reynolds number factor, one by Shah [30], selecting the greater one of the two components with the use of the boiling number Bo and the convective number Co, and another one by Kutateladze [31], combining two components by a power-type asymptotic model. A number of flow boiling

correlations published in the last three decades are only variations of these models.

To make a simple prediction before the experiment, here we choose Chen's model for calculation.

By using the additive concept in principle, Chen [29] formulated the first general correlation for flow boiling heat transfer as

$$h_{tp} = S \cdot h_{nb} + F \cdot h_{sp} \qquad (1-12)$$

Where,

for $1/X_{tt} > 0.1,\ F = 2.35(\frac{1}{X_{tt}} + 0.213)^{0.736}$,

for $1/X_{tt} \leq 0.1,\ F = 1$,

$X_{tt} = \left(\frac{1-x}{x}\right)^{0.9} (\frac{\rho_g}{\rho_f})^{0.5} (\frac{\mu_f}{\mu_g})^{0.1}$,

$h_{sp} = 0.023 Re_f^{0.8} Pr_{0.4} (\frac{k_f}{D_h})$,

$S = 1/(1 + 2.53 \times 10^{-6} Re_f^{1.17})$,

$h_{nb} = 0.00122 (\frac{k_f^{0.79} c_{pf}^{0.45} \rho_f^{0.49}}{\sigma^{0.5} \mu_f^{0.29} h_{fg}^{0.24} \rho_g^{0.24}}) \Delta T_{sat}^{0.24} \Delta P_{sat}^{0.75}$,

Here Chen introduced two dimensionless factors, the suppression factor S and the Reynolds number factor F, to account for the smaller effective superheat due to forced convection as compared to that in a pool boiling case, and for the increase in convective turbulence due to the presence of vapor phase, respectively.

1.7. Conventional research in our laboratory

Nakamura et al. [32] (2014) reported that when compared to conventional solar systems HCPVT system is a system with superior economics in terms of energy collection power, energy conversion efficiency and introduction cost. In addition, a concentrator was designed that could collect sunlight sufficiently at wind speeds of up to 20 m/s and could withstand wind speeds up to 40 m/s. Hara et al. [22] (2016) reported that a three-junction solar cell is very suitable for concentrating photovoltaic system. When concentration ratio up to 200 $xsuns$, the photovoltaic energy conversion is an average of 25.6%. Besides, a micro-channel cooler was attached to the concentrator, and its heat recovery performance was evaluated. Heat recovery efficiency of 53.2% at maximum and 34.7% on average was obtained, and the possibility of simultaneous use of sunlight and heat was shown in experiments, and it was stated

that some contrivance was needed to improve system performance. Zheng et al. [24] (2017) conducted a boiling heat transfer experiment at a heat flux of 11.9 to 46.8 W/cm^2 using a flat tube heat exchanger with a hydraulic diameter of 0.847 mm. It was reported that flow instability appeared when heat flux exceeded 46.8 W/cm^2,that is to say heat sink could not work under that situation. Hamada et al. [25] (2018) reported that there were some flaws in the parabolic dish concentrator composed of mirror. Some of the parts had low reflectivity or even could not reflect the sunlight.

1.8. Objective of study

High concentration photovoltaic system is complicated that mixed a lot of disciplines including electronics, heat transfer, solar energy technology, geography and etc.

In order to realize the co-generation of HCPVT system, from the perspective of heat transfer, this study is dedicated to figure out an appropriate way to cool the solar cell while concentrating. Thus, the parameters concerned with thermal characteristics are discussed in this article. The detailed objectives are as follows.

1. Experiment on the heat transfer coefficient with a high heat flux.
2. Suppress the flow boiling instability in two-phase flow.
3. Figure out the effect of gravity/orientation on the micro-channel exchanger.
4. Apply the solar cell on the heat exchanger and realize co-generation of HCPVT system.

Chapter 2 Experiment on thermal characteristics of radial expanding micro-channel heat exchanger

2.1 Previous work

HCPVT system is a hybrid system which extends the functionality of concentrating photovoltaics (CPV) from simply generating electricity, to providing simultaneously electricity and heat. The utilization of otherwise wasted heat significantly enhances the overall system efficiency and boosts the economic value of the generated power output. An ideal system should consist of a scalable hybrid photovoltaic – thermal receiver package, cooled with an integrated high performance microchannel heat sink.

Actually, the experiment of HCPVT system has been operated for several months, an experimental loop, as shown in fig.2.1, has been established. The receiver package was mounted on an outdoor (on the rooftop of the environment building) active-tracking system. The sunlight was concentrated on the receiver with a diameter of 2 m, focal length of 1.2m parabolic dish concentrator having a concentration ratio of approximately 1000. The parabolic dish was located on a two-stage tracker to pursuit the movement of the sun enabling consistent measurements for an extended time period. As seen in fig2.2, The direct solar radiation was recorded by a pyranometer fixed on the concentrator and global radiation was measured by a pyranometer on the top of building.

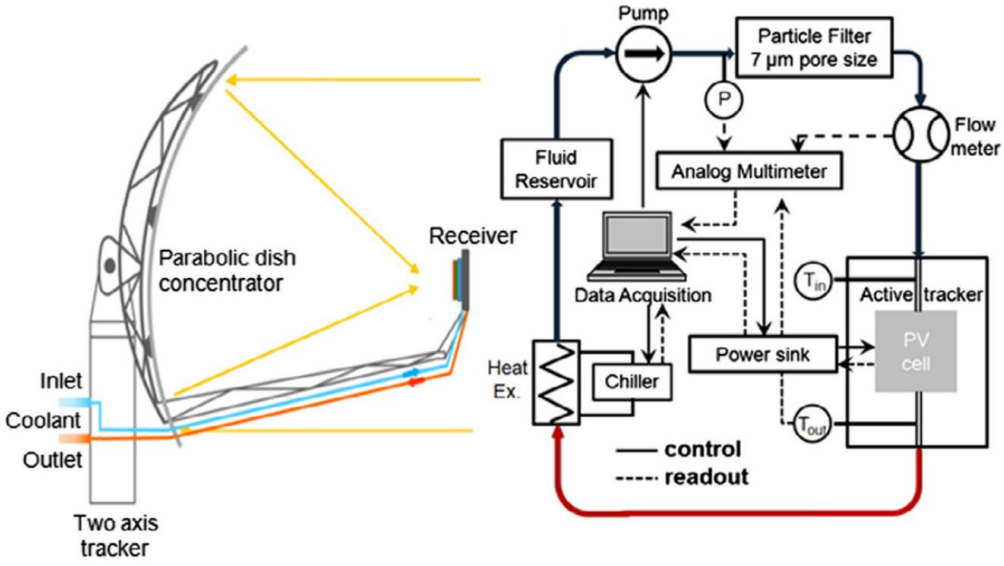

Fig.2.1: Scheme of the parabolic dish concentrator and the experimental outdoor test facility

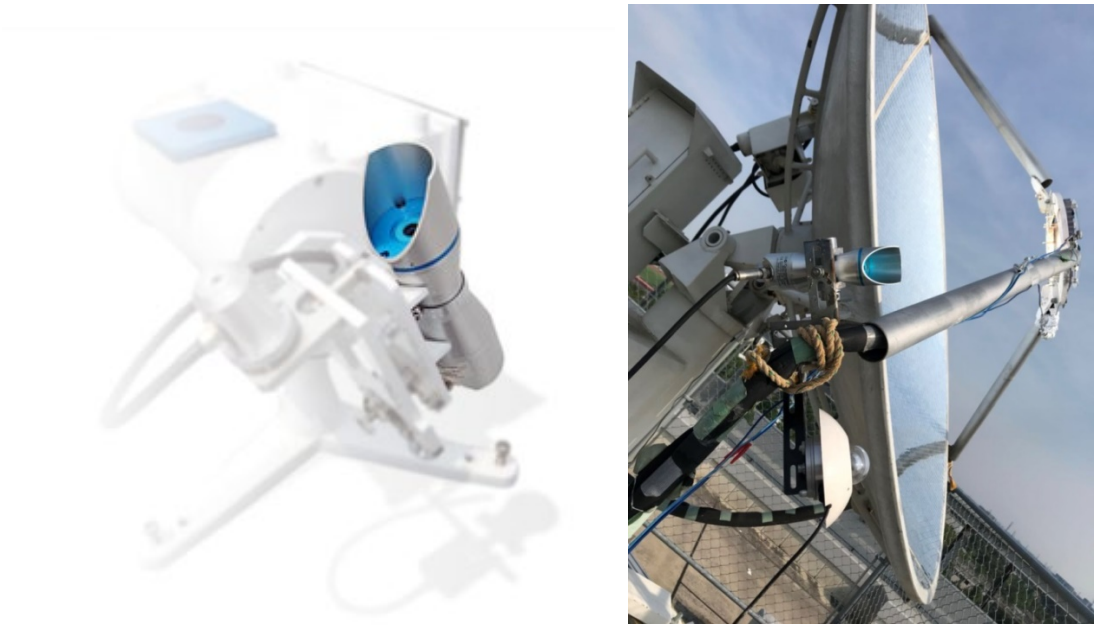

Fig.2.2: Pyranometer for recording solar radiation

A micro-channel heat sink was used in the HCPVT system and single-phase flow convection heat transfer was utilized to cool the solar cell. Fig.2.3 is the solar radiation and inlet/outlet temperature as a function of time. The testing was from 12:00 at noon and last 4 hours till the 16:00, the solar radiation is linear to the time, that is to say the testing condition is stable and reliable. Keeping the inlet temperature in about 36℃ is to realize a stable flow convection condition.

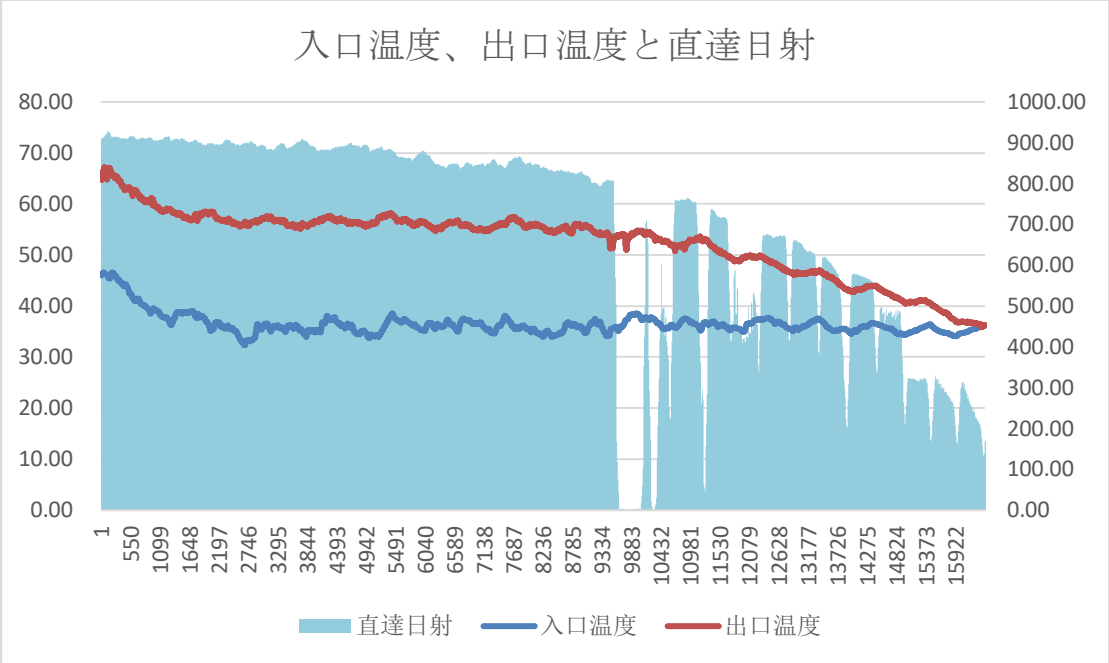

Fig.2.3: Fluid temperature and solar radiation

To predict the thermal characteristics, the conventional convection flow heat transfer coefficient is calculated by,

$$t_f = \frac{T_{in} + T_{out}}{2} \quad (2-1)$$

$$u = \frac{Q}{A} \quad (2-2)$$

$$\mathrm{Re} = \frac{ud}{V_f} \quad (2-3)$$

$$Nu = 1.86\left(RePr\frac{d}{l}\right)^{\frac{1}{3}} \quad (2-4)$$

$$\mathrm{Nu} = \frac{hd}{\lambda} \quad (2-5)$$

$$H = Nu \times \frac{\lambda}{d} \quad (2-6)$$

$$\Delta T = \frac{q_{eff}}{H} \quad (2-7)$$

$$T_{he} = T_{in} + \Delta T \quad (2-8)$$

Where V_f is Viscosity coefficient, P_r is Prandtl number, ρ_f is water density and d is Channel Hydraulic diameter.

Fig.2.4: Photo of concentration and weather of experiment

The weather condition and focal spot were shown as fig.2.4, it means the experiment was conducted under a stable heat flux situation. Unfortunately, the heat transfer performance of single-phase is calculated by $1971\ W/m^2K$ and the temperature of surface of heat sink would be calculated by 202℃ which is impossible to cool down the solar cell. The result was verified

by thermography, as shown in fig2.5. As a consequence, poor heat transfer performance by flow convection heat transfer in such high heat flux is conducted.

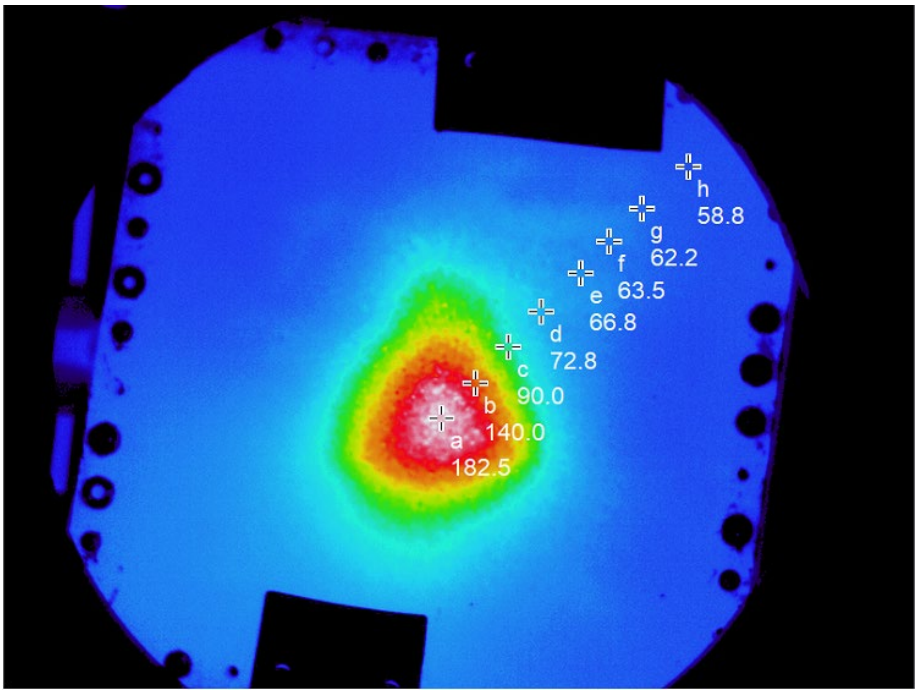

Fig.2.5: Thermography of the surface temperature of heat sink

Obviously, the wall temperature (182.5°C) was extremely too high for solar cell to work.

2.2 A design of new-type micro-channel exchanger

To improve the heat transfer performance and ensure the solar cell a good working condition to realize the co-generation of HCPVT system. A new-type radial expanding micro-channel heat sink was designed.

Novel heat sink utilizing two-phase cooling attracts increasing attentions owing to the high heat transfer capacity and convenient assembly [36]. However, the application of two-phase heat sinks in engineering field confronts intricate issues of flow maldistribution [37] and flow instability [38]. Attributed to the enhanced effect of surface tension in small scaled space, isolated bubble flow, elongated bubble flow and annular flow are the main flow patterns observed in microchannels [39]. Bubbles inside channels evaporate fast and elongate towards both sides, interim vapor blockage and succeeding pressure peak are induced [40], which causes reverse flow or even local dry-patch [41]. Violent fluctuations in wall temperature, inlet mass flux and pressure caused by flow instability have been reported in previous researches. Usually, unstable flow boiling leads to an early heat transfer deterioration at low vapor quality. It is

concerned that the flow instability often occurs in parallel array micro-channels.

To relieve the instability of two-phase flow, a brand-new design of micro-channel is introduced. An expanding channel heat sink is designed for two-phase flow heat exchanger, as seen in fig.2.6.

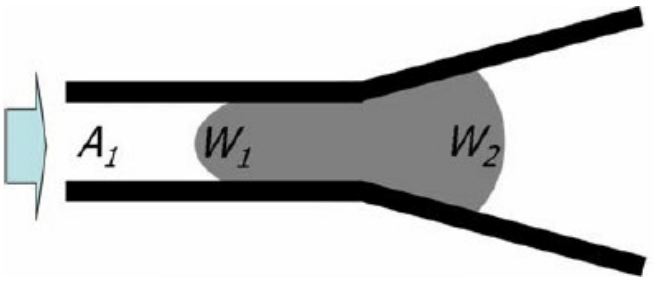

Fig.2.6: Expanding channel

It displays the schematic sketch of a single bubble's elongation in an expanding channel, W_1 and W_2 is the diameter of channel cross-section area. Compared to straight channel, the expanding channel cross-section produces a net surface tension on an elongated bubble, which assists the removal of vapor and eases the vapor blockage in channels. For one channel, the net surface tension force can be illustrated by Eq.2-9.

$$\Delta P_s = \sigma\left(\frac{1}{W_1} - \frac{1}{W_2}\right) \qquad (2-9)$$

Where σ is the surface tension of liquid. Eq.2-9 shows a force pushing the vapor out of the channel.

To suppress the flow reversal, we proposed to add cut-off structures to interrupt the backward expansion of vapor in the channel. Fig.2.7 shows the structure of cross-cutting grooves perpendicular to the flow direction, with the help of cut-off structures, long bubbles would be broken into several pieces which leads to a lower pressure drop and also could redistribute the flow rate among the micro-channels. Thus, the flow instability can be hugely suppressed.

Fig.2.7: Cross-cutting structure

With these two conceptions, the new-type micro-channel heat sink was designed. The channel was combined with expanding and cut-off structure, as seen in fig.2.8, along the flow direction there is a bigger space for bubbles to grow and cut-off structure, shown in fig.2.9, can break a long bubble into several parts.

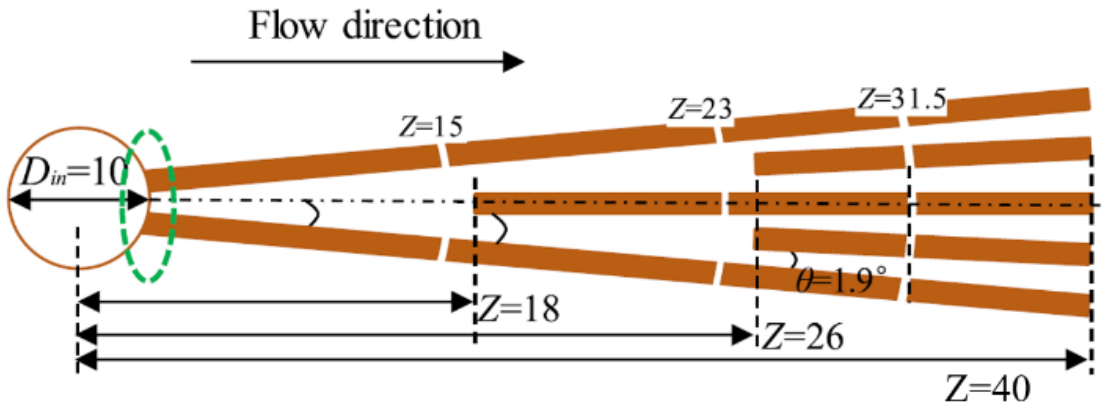

Fig.2.8: Sketch of radial microchannel heat sink

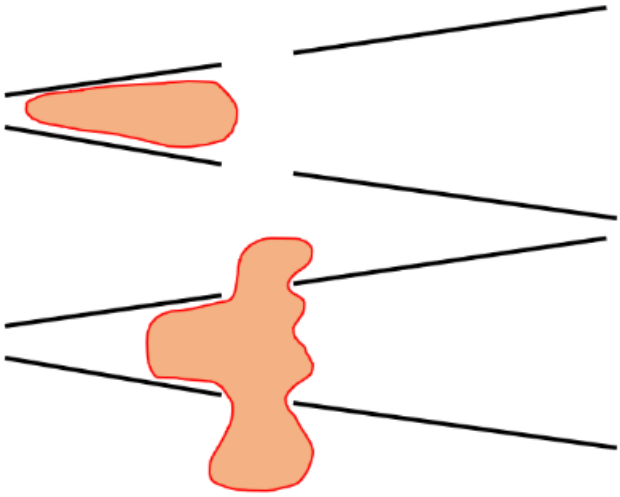

Fig.2.9: Sketch of cut-off in microchannel

The radial expanding micro-channel heat sink was introduced by Hong sihui in 2018 [42].

Compared with parallel array channel, the inlet is set at the center of the heat sink which makes the flow rate distribution more uniform. The expanding channel gives a flatter space for bubbles to grow. In that way, the flow instability could be greatly suppressed and the heat transfer would be more stable and efficient.

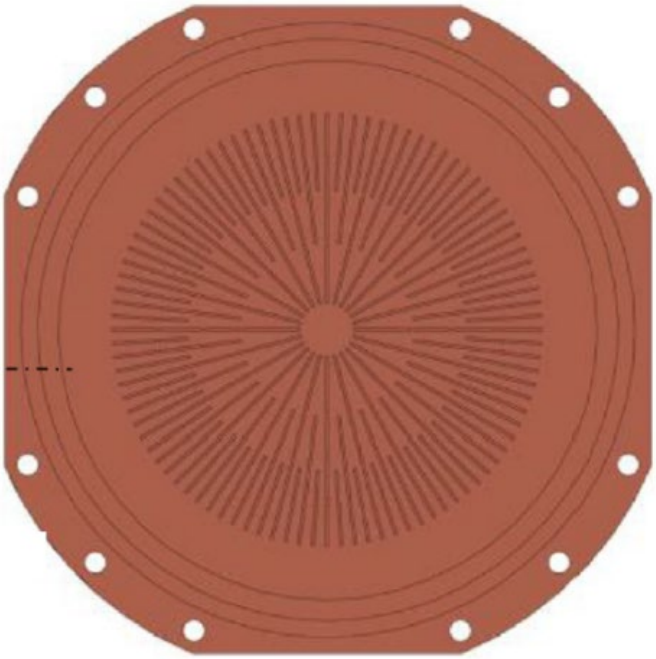

Fig.2.10: Sketch diagram of radial expanding micro-channel heat sink

2.3 Experimental setup

The schematic diagram of experimental loop is shown as Fig.2.11. Deionized water was used

as the working fluid. The inlet liquid was supplied by a micro gear pump (MICROPUMP GJ-DB380.A), as shown in fig.2.12, and the flowrate was measured by a mass flow meter (OVAL ALTI mass II CA001) before flowing into test section. The needle valve in the loop was used to adjust the inlet mass flowrate. To realize two-phase flow boiling heat transfer, before flowing into test section, the liquid is heated by a thermostatic bath preheater, as seen in fig.2.13. The temperature of inlet subcooled liquid was regulated at 84.71 ± 0.5℃ because it is the maximum capacity of bath preheater. It is true that the less subcooling is better for two-phase flow heat transfer but it is evidenced that 15℃ subcooling does not have much influence on that. The two-phase flow outflowed the test section was cooled down by a plate heat exchanger type condenser before the tank.

Fig.2.14 is a photo and diagram of the heater, in which a copper block was inserted six electrical heating rods. The surface in contact with heat sink was coated silicon grease to enhance heat transfer. To evaluate the heat flux, two small holes were drilled below the top of the surface and inserted thermocouples, as seen in fig.2.14 (b). With the help of thermal conductivity of copper and temperature difference between T1 and T2. Heat flux could be calculated by Eq.2-10:

$$q_{eff} = \frac{T_2 - T_1}{\frac{\lambda}{L}} \qquad (2-10)$$

Where λ is thermal conductivity and L is the thickness of position 1 and position 2.

In a test section, six electrical heating rods were used as an independent heat source for heat exchanger, and the heating load was provided by a power meter Hioki 3333, as shown in fig.2.15, the heat could be alternated from 0 to 1850 W. The area of top of the copper block is the same as the heat exchanger. The test section was kept horizontal. The test section and all connecting pipes were wrapped with thick asbestos fabric for thermal insulation. The temperatures at the inlet and outlet were measured by K-type thermocouples. To calculate the saturation temperature of the system, it is necessary to measure the pressures at the outlet. The pressures at the inlet and outlet were measured by pressure sensor switch gauge (NAGANO KEIKI KP-15), the outlet pressure was maintained at 107.2 ± 1 kPa by the test bench, thus the corresponding saturation temperature was within 101.5 ± 0.5 _C. All the thermocouples and pressure sensor were recorded in a high-speed analog measurement unit NR-HA08, as shown

in fig2.16, the recording frequency could be 500Hz if it is necessary. The input heat load Q varied from 1000 to 1850 W, and the inlet mass flowrate m ranged from 120g/min to 300 g/min.

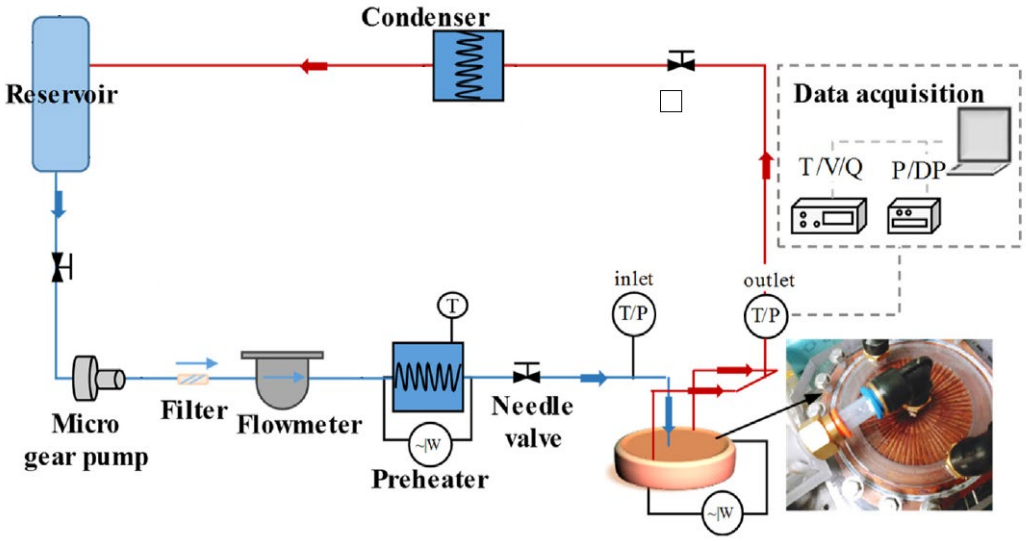

Fig.2.11: Experimental loop

Fig.2.12: Micro gear pump

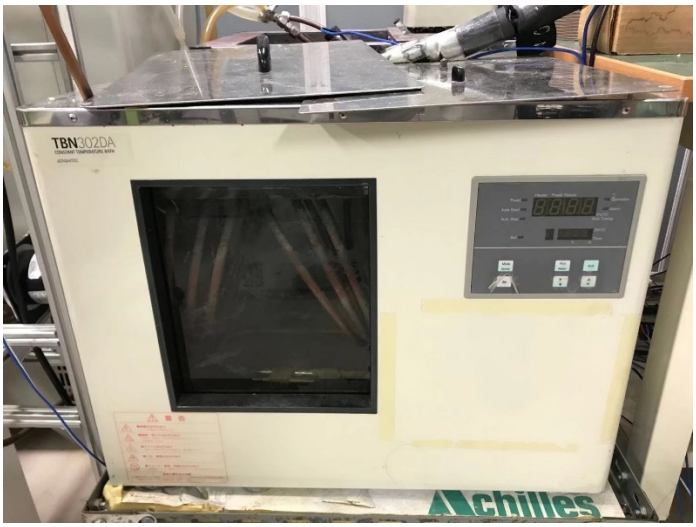

Fig.2.13: Thermostatic bath preheater

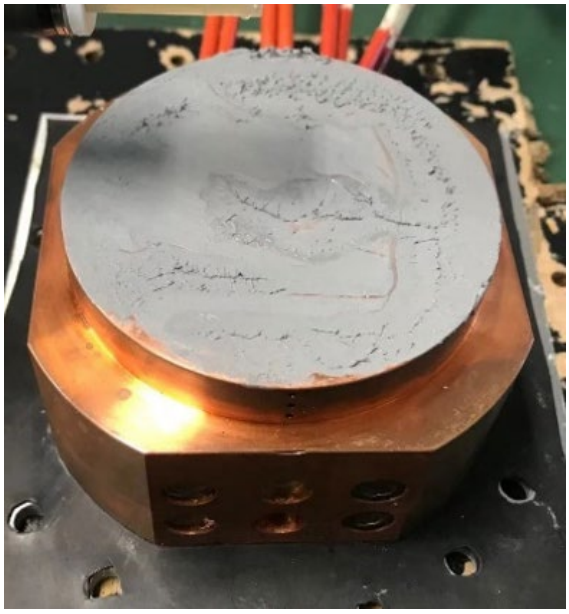

(a) Copper block heater

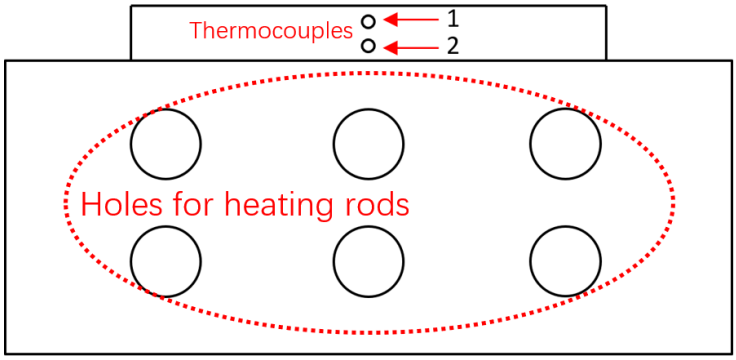

(b) Sketch of copper block heater

Fig.2.14: photo and sketch of heater

Fig.2.15: Photo of power meter

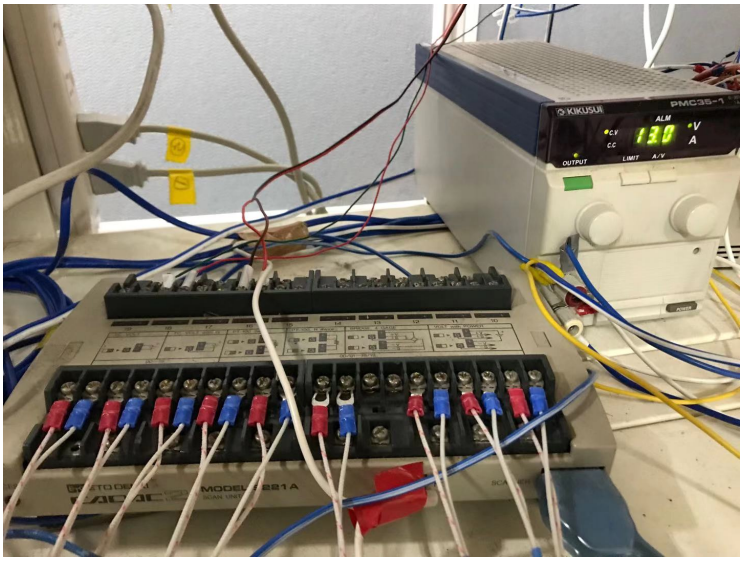

Fig.2.16: High speed data logger

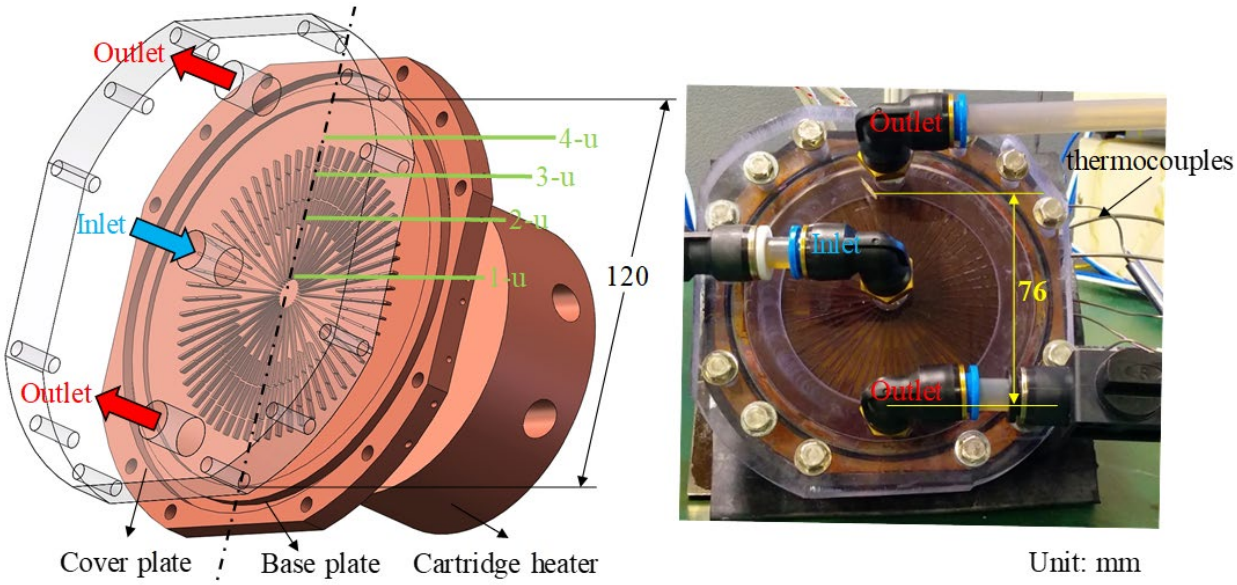

(a) Test section and thermocouples' location (b) Photo of test section

Fig.2.17: Schematic diagram of experimental set-up

Heat exchanger is consisting of a copper base plate (7 mm in height), and a polycarbonate cover plate (30 mm in height) for the convenience of visualization, as shown in fig.2.17 (b). An O-ring was used for sealing.

All of the micro-channels in test section are 1.5 mm in height, and the thickness is 0.5 mm. Cut-off structure contributes to easing unexpected inverse flow and making flow more even in each channel.

Shown as Fig.2.17 (a), 8 test points were symmetrically arranged in each HE to detect the distribution of wall temperature along the radial direction. The thermocouples were 5 mm beneath the bottom surface of channel. From the upper of heat sink, the thermocouples were named 4-u, 3-u, 2-u, 1-u and from the bottom of the heat sink, the thermocouples were named 4-d, 3-d, 2-d, 1-d. All the measuring sensors were calibrated before testing. The precision of thermocouples was calibrated by high precision standard thermometer to ±0.10 K. The maximum accuracy of measured geometric dimensions is 0.05 mm.

2.4 Suppression of two-phase flow instabilities

Flow boiling instability is a critical issue that should be taken into consideration during the design of micro evaporators. It might have a dramatic effect on the overall system performance. Once the flow becomes unstable, all system parameters such as mass flow rate, pressure and

temperature oscillate with large amplitudes. These amplitudes can be as high as 36 K for wall temperature, as found by Wang et al. [73], and 992.4 kg/m2 s and 60 kPa for mass flux and pressure drop, respectively, as found by Fu et al. [74]. Thus, the local time averaged heat transfer coefficient may be strongly influenced by these fluctuations.

Along the flow direction, temperature of flow is rising up. When it reaches the saturation temperature, phase-change begins and bubbles come from the fluid. As shown in fig.2.18, different flow regimes state in micro-channel along the flow direction. Therefore, the local flow boiling heat transfer coefficient is also changed simultaneously.

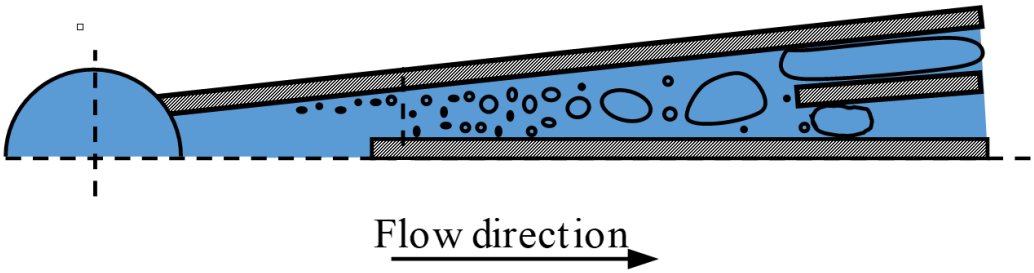

Fig.2.18: Schematic drawing for different flow regimes in micro-channel

While vapor quality is getting bigger and bigger, evaporation on the boundary layer is becoming intense which contributes to local boiling heat transfer coefficient. However, on the other hand, boundary layer becomes thinner and it is possible to observe dry-out in microchannel which is fatal to heat transfer.

To suppress dry-out in micro-channel, a technology is introduced in micro-channel heat sink. A copper foam, shown in fig2.19, is introduced.

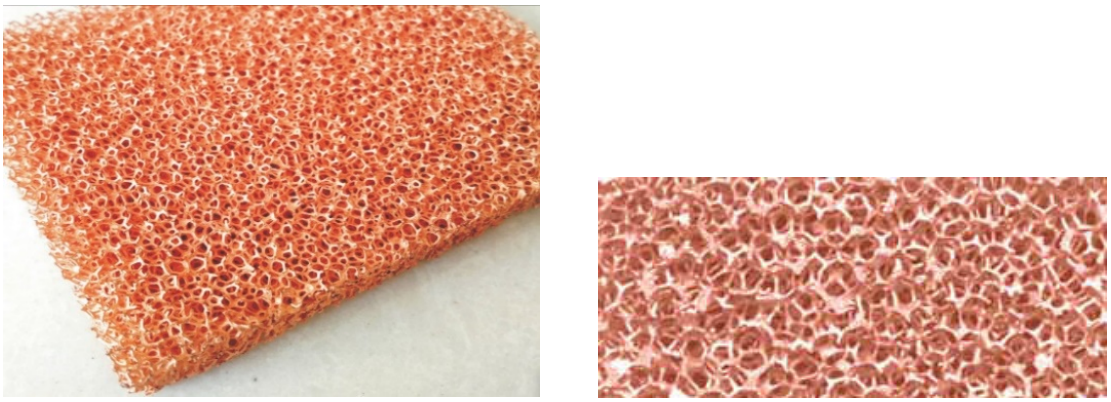

Fig.2.19: Copper foam

The physical properties are listed in Table2.1,

Table2.1: Physical properties of foam copper

Density	cell size	*Void ratio*
8.96g/cm^3	10 to 20 pores/cm	20%

To avoid dry-out in micro-channel, replenish fluid and keep channel wet is a must. In that way a copper foam, which is a cellular structure consisting of copper with gas-filled pores comprising a large portion of the volume and having a high porosity about 80%, is placed between the heat sink and cover plate, as shown in fig.2.20.

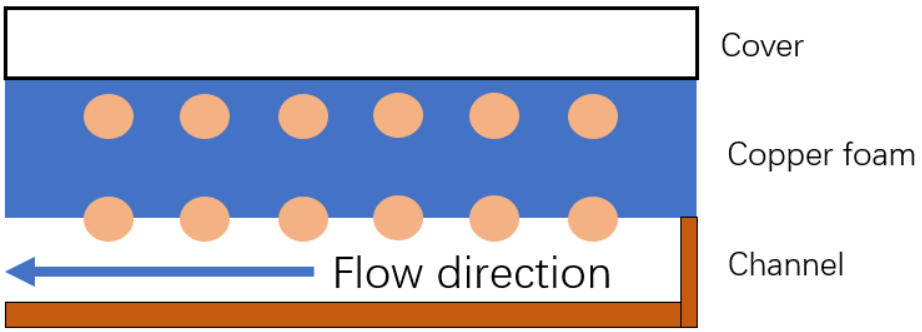

Fig.2.20: A sketch diagram of copper foam

Copper foam is capable to let fluid flow into the micro-channel but also can store a part of liquid between heat sink and cover plate. When the channel becomes liquid-deficient, the pressure diffidence can draw the water from water-storage layer into the micro-channel to keep channel wet permanently.

2.5 Test procedure and data processing

The heat transfer capacity of HE is evaluated with the average saturated boiling heat transfer coefficient $h_{average}$, defined as Eq.2-11, where q_{eff} is the effective heat flux in terms of the footprint heating area, defined as Eq.2-12. $T_{w,aver}$ is the average wall temperature in saturated region, and T_{sat} is the saturated temperature of working liquid under the outlet pressure.

$$h_{aver} = \frac{q_{eff}}{T_{w,aver} - T_{sat}} \qquad (2-11)$$

$$q_{eff} = \frac{Q}{\pi \cdot L^2} \qquad (2-12)$$

Where Q is the energy from heater, L is the radius of heated surface.

One thing to mention is that calculated heat transfer coefficient does not involve inlet region because the heat transfer in this region might be dominated by single-phase forced convection.

However, the area ratio of the inlet region is as small as 1.56% and mass flow is so little that subcooled fluid could be heated to saturation instantly, the heat transfer characteristics in HE almost dominated by flow boiling. Thus, the single-phase heat transfer can be omitted in this research.

2.6 Theoretical analysis on thermal characteristics

Significant differences in transport phenomena have been reported for micro (mini) -channels as compared to conventional ones. Among various factors distinguishing flow boiling in mini-channels from that in conventional channels there are two most important to our understanding.

1) The first one is due to the effect of surface tension. As pointed out by Triplett et al. explained that due to the dominance of surface tension, stratified flow is essentially absent, slug (plug) and churn flow patterns occur over extensive ranges of parameters, and the slip velocity under these flow patterns is small. In such flow patterns, most of the liquid flows in a thin liquid film along the wall and the vapor flows mostly in the core of the channel due to the effect of surface tension. Since the channel size is small, it can be anticipated that at low flow rates the thin liquid flow is of characteristics of laminar flow.
2) The second one is due to the effect of evaporation. As explained by Kandlikar, the effect of evaporation on flow pattern transitions is considered to be quite small in conventional channels. This is one of the reasons why the flow pattern studies on adiabatic gas–liquid systems could be extended to diabatic systems. In mini-channels, however, the effect of evaporation could be quite significant. It alters the pressure drop characteristics. For instance, an acceleration pressure drop component could be quite large at high heat and mass fluxes due to the small channel dimension.

Traditional heat transfer coefficient correlations for saturated boiling with the liquid-turbulent and gas-turbulent flow may not be suitable in principle to predict heat transfer coefficients in micro-channels due to the possible effect of liquid flow laminarization. Therefore, the effect of the flow channel size on the flow boiling heat transfer should be carefully examined in detail. Although many analytical and experimental studies related to flow boiling heat transfer in a micro-channel have been performed for the past decades, in the current

status of this subject, sufficient systematic and accurate data bases are still unavailable to understand flow boiling characteristics in a micro-channel, and a reliable heat transfer coefficient correlation applicable to a wide range of conditions in micro-channels has not been developed yet.

The heat transfer coefficient in micro-channel is a complicated issue which has been researching yet. That is to say, the experiment is an important way to evaluate the thermal performance of heat exchanger.

2.7 Experiment of heat transfer

In order to figure out the relationship between heat flux and heat transfer coefficient, the thermal performance of the proposed radial expanding micro-channel heat exchanger under various working conditions is evaluated, as shown in table.2. T saturation is calculated by outlet pressure and T inlet is controlled by preheater at 82±1℃. With constant mass flow T in and T saturation, turning heat flux from 220,106 W/m² up to 422,424 W/m² .

Table.2-2: Experiment conditions

	Test-1	Test-2	Test-3
Mass flow g/min	300	300	300
Heat flux W/cm²	22.0106	33.0822	42.2424
T in ℃	84.1	82.3	84.7
T saturation ℃	101.2	101.7	101.8

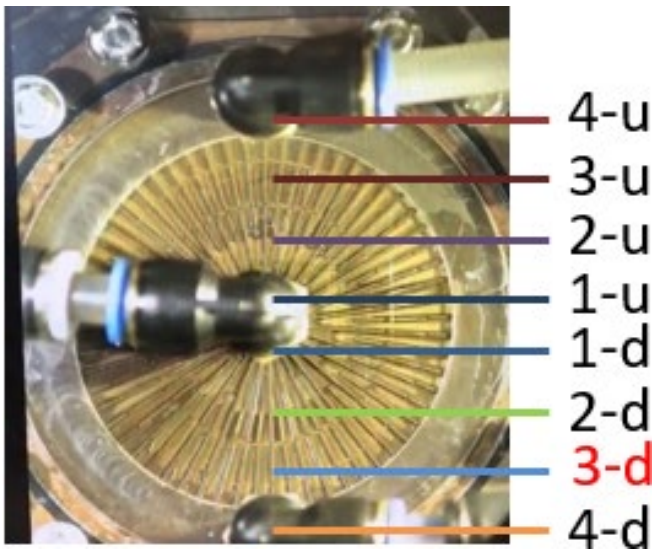

Fig.2.21: 8 points to measure the surface temperature of heat exchanger

Fig.2.21 shows the position of 8 measurements to detect the surface temperature of heat exchanger, from the top till the bottom, there are 4-u, 3-u, 2-u, 1-u, 1-d, 2-d, 3-d, 4-d.

Fig.2.22 shows the wall temperature as a function of time for radial expansion heat sink. As seen in the figure, eight thermocouples are set on the surface of heat sink. Temperature of each working condition is stable and have a difference temperature distribution on the heat sink surface. Among all of the measurement points, T 1-d and T 1-u are the lowest in each test because they are closer to the inlet. That is to say, heat transfer characteristic on that place is dominated by single phase convection, the low surface temperature does not mean a good heat transfer performance because of a great temperature difference between subcooled fluid and surface temperature. Besides, the reason why temperature distribution is not an axisymmetric figure is that heat sink is over a long period of use. Surface characteristic is not the same everywhere, some flaws on the 4-u might cause an abnormal wall temperature.

The highest wall temperature is increasing with the heat flux from 105.5℃ to 112℃, however T 4-u is almost located at the outlet, it is unfair to judge the performance of heat sink with that, on the contrary T 3 is a good measurement point which is used to calculate the heat transfer coefficient. Also, when it comes to particle application, solar cell is more likely to set on the central of heat sink to ensure a maximal energy conversion efficiency because the concentration ratio is at its maximum at the center of focal.

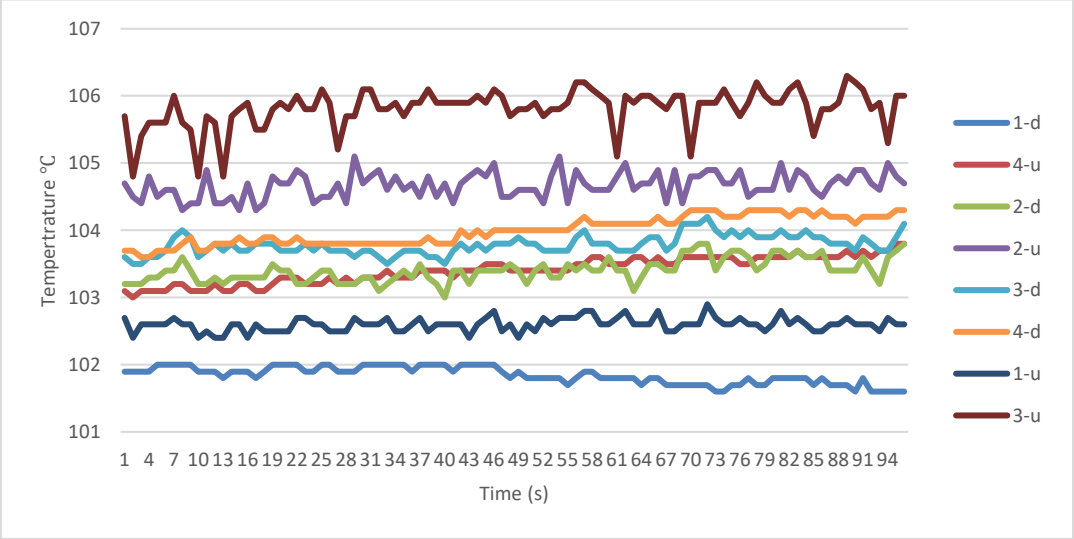

(a) q_{eff}:22w/cm^2,Average x_{out}:0.05, T_{in}:84.1℃, T_{sat}: 101.2℃

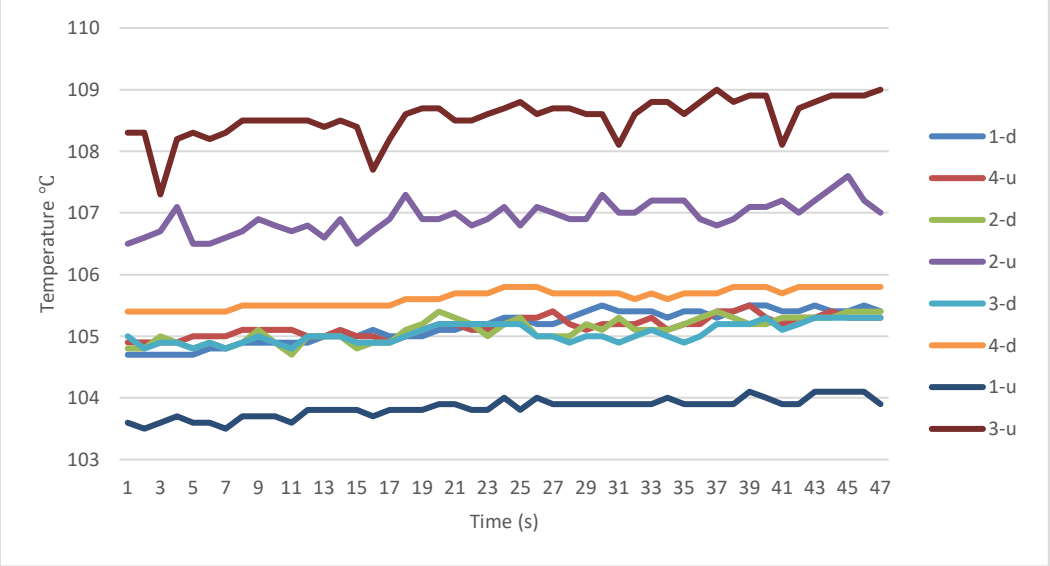

(b) q_{eff}:33w/cm^2,Average x_{out}:0.1, T_{in}:82.3℃, T_{sat}: 101.7℃

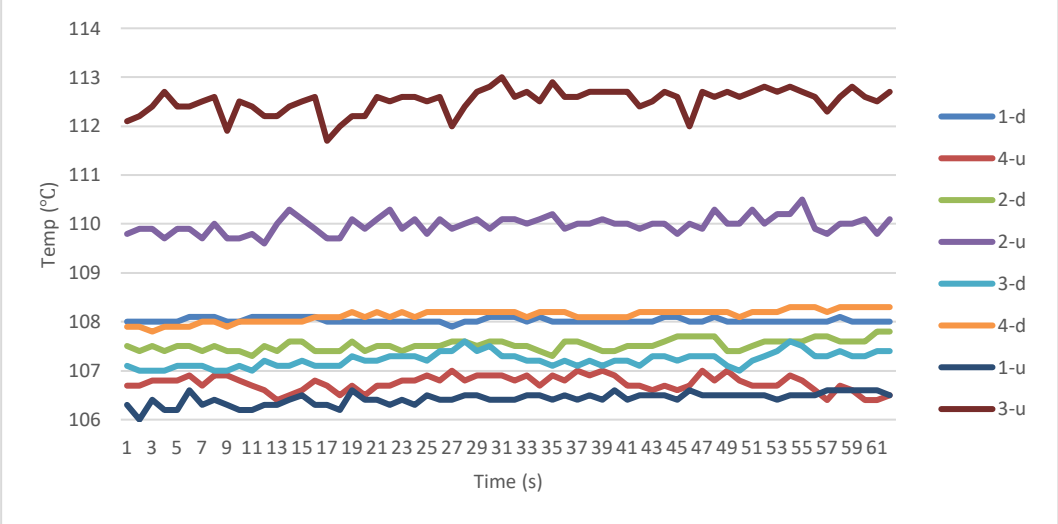

(c) q_{eff}:42w/cm^2,Average x_{out}:0.13, T_{in}:84.7℃, T_{sat}: 101.8℃

Fig.2.22: Temperature distribution of 8 measurement points of HE at mass flow: 300g/min,

To judge a heat exchanger, heat transfer performance is mostly concerned. Fig.2.22 shows the heat transfer coefficient as a function of heat flux for the test section. As seen in the figure, the heat transfer coefficient linear increases with heat flux obviously and reaches as high as 85,000W/m^{2}K when heat flux is 42W/cm^{2}K which is the maximum capacity of heater in laboratory. The result is constant with the flow boiling curve, shown in fig.2.23, it means a stable nucleate boiling occurred in test section. Besides, this thermal characteristic is ideal for solar system use.

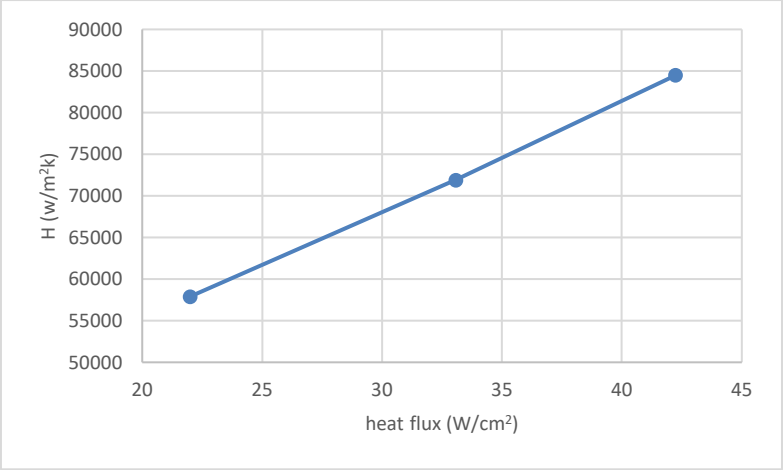

Fig.2.22: relationship between heat transfer coefficient and heat flux

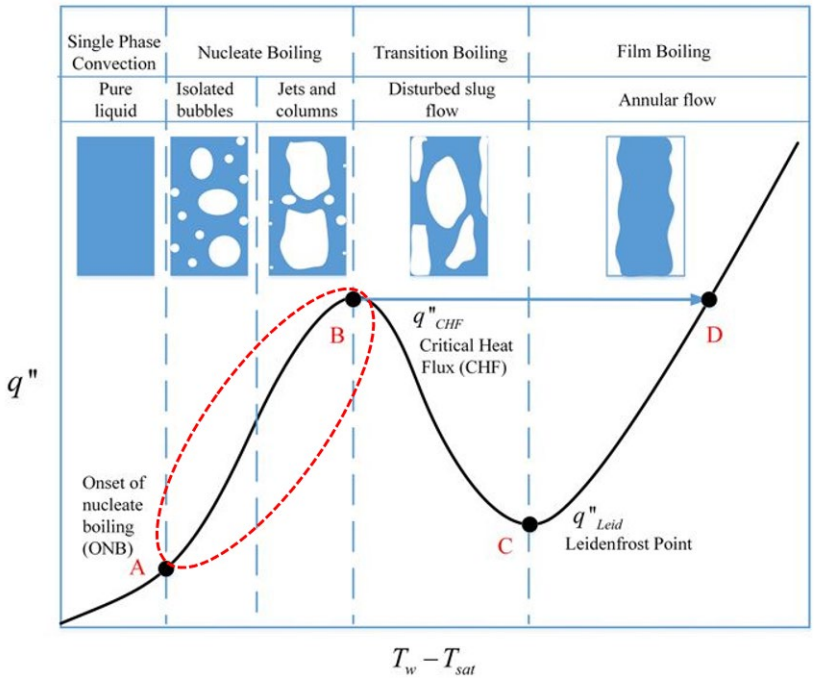

Fig.2.23: Flow boiling curve

When it comes to practice application, installed in photovoltaic system, the working condition of 42W/cm^{2}K heat flux tested in laboratory is equivalent to 761 $xsuns$ concentration ratio with a direct normal radiation of 600W/m^2. When radiation increases to 1000W/m^2, the heat flux concentrated on the surface of heat sink will rise which also leads to a higher thermal performance.

Besides the heat flux, vapor quality and mass flow are also significant parameters when judging a heat exchanger. Fig.2.16 (a) (b) (c) (d) (e) shows wall temperature as a function of vapor quality, in all of the working condition, heat sink was kept in the same heat flux, T in and saturation temperature was nearly the same. By changing mass flow, we can get a controllable outlet vapor quality.

As seen in the figure, the highest wall temperature is the 3-u about 113℃ and does not basically change with vapor quality. It is abnormal no matter by theory or imagination. The reason why the temperature of 3-u is always the highest is because the structure of the copper block heater. According to fig.2.14, the copper block was excavated six holes for heating rods to insert and the positions of rods were beneath the 3-u and 3-d, that is why the temperature of 3-u is always the highest. Also, the heat sink has been using for about two years, the roughness of surface and the structure of micro-channel might have been changed, so the temperature distribution is not symmetric. In other word, the temperature curves could show an overall thermal characteristics of heat exchanger but the details might be accounted for flow boiling mechanisms or uncertain factors, there are lots of work to do.

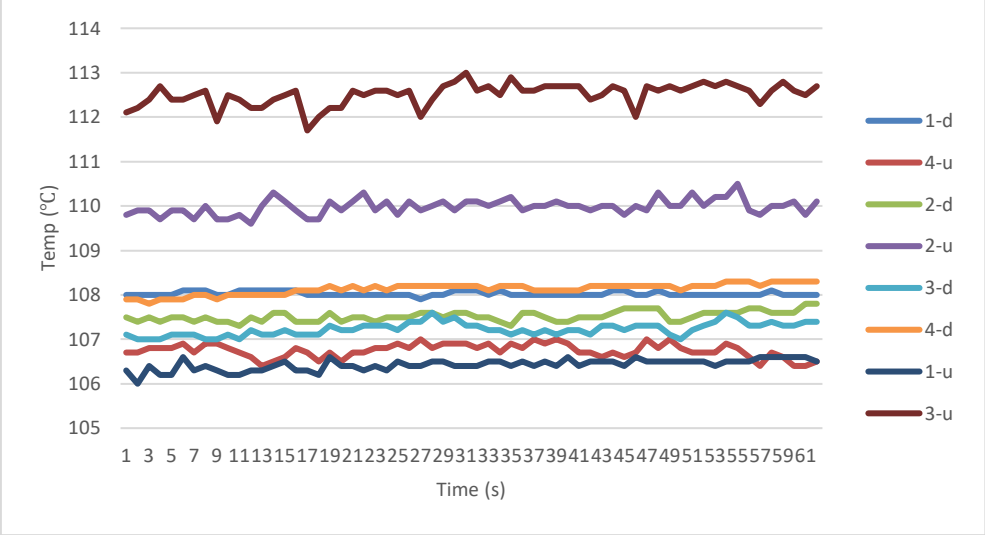

Mass flow: 300g/min, x_{out}: 0.13

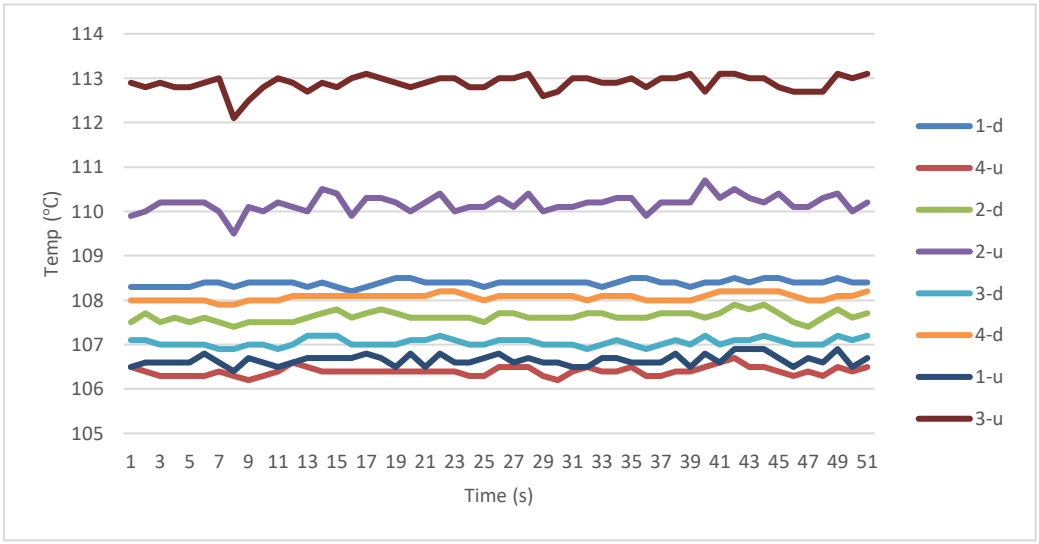

(b) Mass flow: 250g/min, x_{out}: 0.166

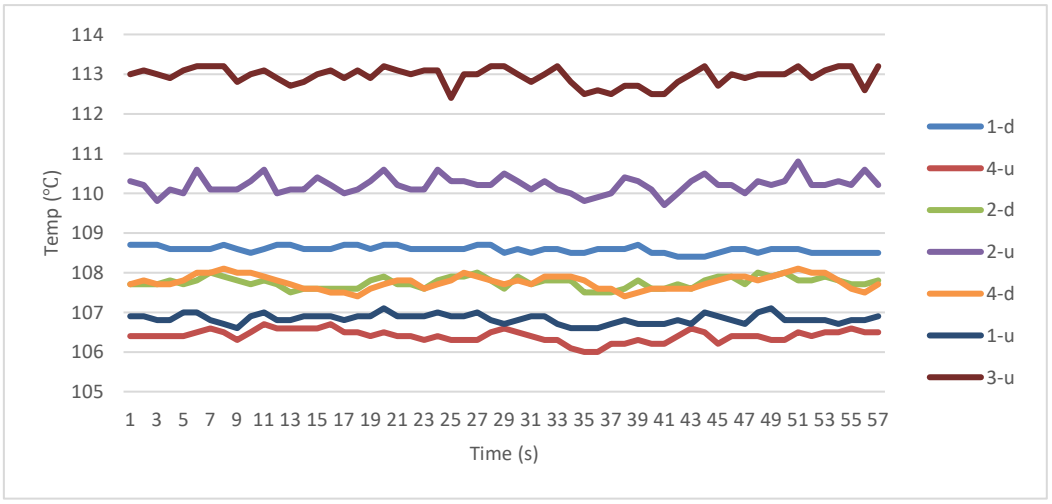

(c) Mass flow: 200g/min, x_{out}: 0.214

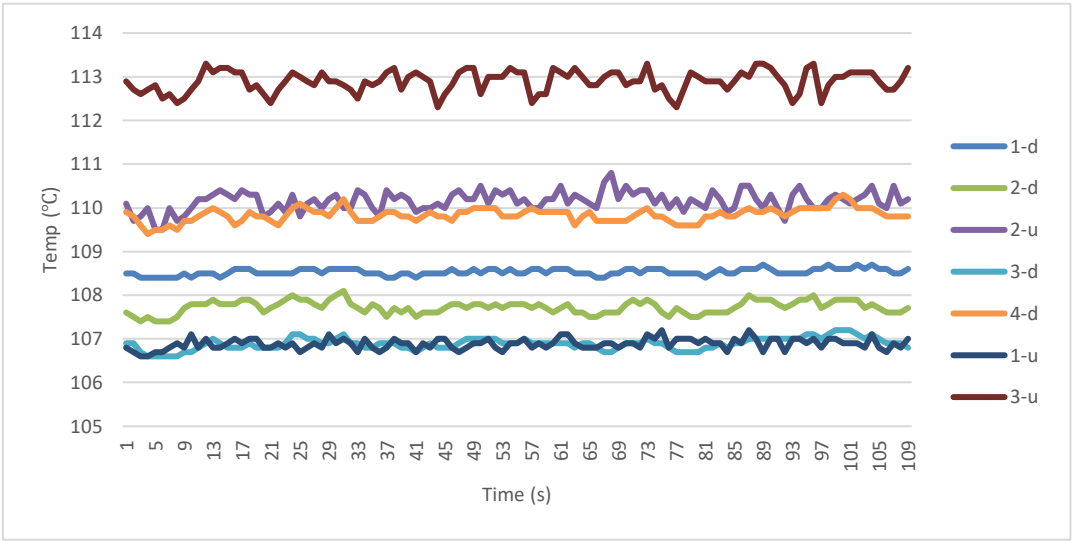

(d) Mass flow: 150g/min, x_{out}: 0.296

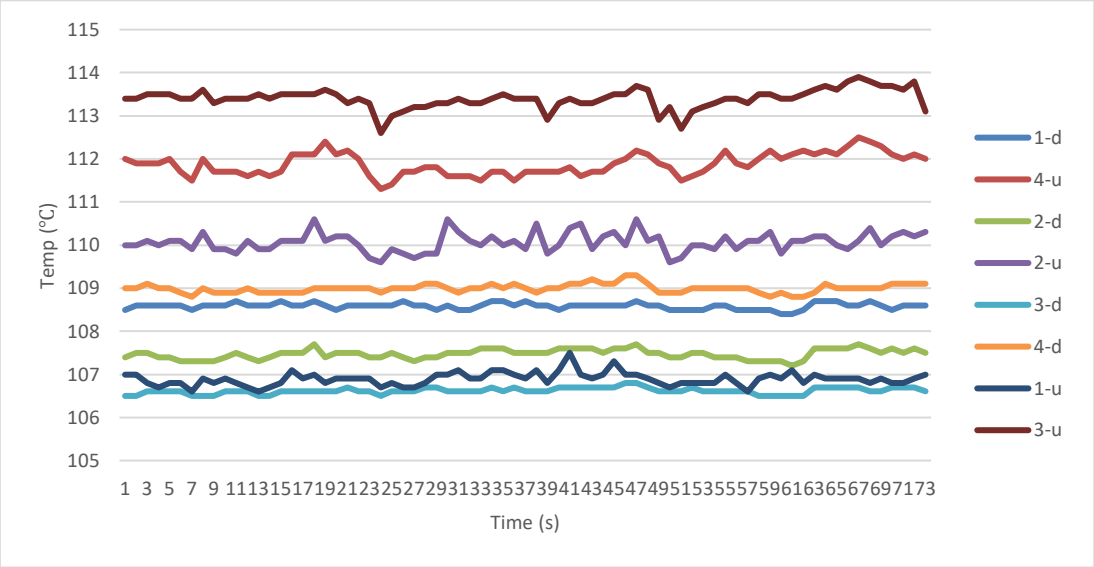

(e) Mass flow: 120g/min, x_{out}: 0.378

Fig2.16: Temperature distribution of 8 measurement points of HE at heat flux 42W/cm^2

Fig.2.17 is plot of the heat transfer coefficient as a function of vapor quality for the test section. As seen in the figures, the heat transfer coefficient is stable when vapor quality is increasing.

An experiment was also performed under higher vapor quality condition, but if x is above 0.4 the wall temperature would rise rapidly and dry-out could be observed in the micro-channel. This could be because the bubble creation frequency is too high and too many bubbles occupy the channel wall, which may result in a suppression of the nucleate boiling. The flow regimes in this region were observed to be churn and annular. If the evaporation was too intensive, the boundary layer would be broken and cause dry-out in the channel. In that way, although the heat transfer coefficient is independent with vapor quality, it is need to ensure enough fluid flow into the channel and keep the wall wet all the time.

Besides, the heat transfer coefficient can be reached nearly 100,000 W/m^2K when heat flux is 42 W/cm^2 which is equivalent to 600 W/m^2 solar radiation in HCPVT system. It can be inferred that the surface temperature of HE is only 110℃ in that situation which is safe for installed a solar cell to realize energy conversion.

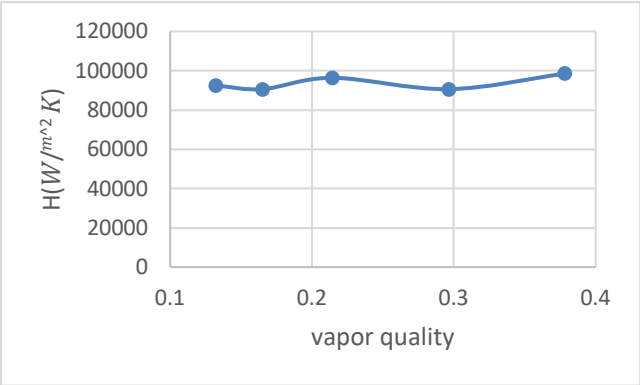

Fig.2.17: Heat transfer coefficient as a function of vapor quality

Combined fig.2.15 with fig.2.16, the heat transfer coefficient increases with heat flux and does not change clearly with vapor quality when x is in the range of 0.13-0.378.

That is to say, the independence of the heat transfer coefficient on vapor quality with increasing mass flow is ideal for a photovoltaic system. If the solar radiation becomes intensive, heat flux concentrated on heat sink would also be rising. High heat flux brings better heat transfer performance, which means the solar cell is capable of cooled whenever on a cloudy day or a shining day. Furthermore, the independence of the heat transfer coefficient on vapor quality makes the control of HCPVT system much more simply because there is no need to adjust mass flow rate when radiation is changed, thermal performance is nearly the same with mass flow at a range of 120g/min to 300g/min which makes the HCPVT system more independent and smart.

2.8 Conclusion

From a theoretical perspective, nucleate or convective or a combination of the two regimes can characterize two-phase flow boiling heat transfer in tubes/channels. In nucleate boiling, the heat transfer coefficient is a function of the heat flux and system pressure but does not depend on vapor quality and mass flow. In the convective mode, the heat transfer coefficient is strongly dependent on mass flow and vapor quality but independent of heat flux.

To guard conclusion of experiment and prove its reliability, it is necessary to compare the result with other similar researches.

From the experiment on thermal characteristic of radial expansion micro-channel exchanger, we conclude that heat transfer coefficient remains a high level about 100,000 W/m^2K during

the test and is independent on vapor quality at a range of 0.13-0.37. The surface temperature can be cooled at nearly 110℃ while saturation temperature is 101.2℃, that is to say the temperature difference between wall and fluid is only 8.8℃ under a heat flux of 42 W/cm^2. That means radial expansion micro channel HE has a great capability of heat transfer and proves that it is feasible to cool solar cell with that HE.

Chapter 3 Experiment of effect of gravity on radial expansion microchannel HE

3.1 The effect of gravity

Miniaturization of electronic devices has led to an increase in power density which poses severe challenges to maintain the operating temperatures within the safe limit [59–61]. Conventional single-phase cooling systems with air/liquid coolants are insufficient to meet this demand [11,62]. Accordingly, there is a need to develop advanced thermal management solutions capable of dissipating high heat flux within minimal temperature budgets. In this regard, flow boiling in microchannels is envisioned as a viable solution to dissipate high heat flux in excess of 10 MW/m2. However, practical implementation of flow boiling in microchannels is limited due to two-phase flow instabilities encountered at high heat fluxes.

As a kind of instability, rapid bubble growth and expansion in the upstream and downstream sides of the channel. This explanation was reported by [75–79]. At this condition, it was observed by all the above that the bubble remains stationary for a very short time period with small axial oscillations or slides slowly forward. Accordingly, evaporation of the thin liquid layer underneath the bubble during this period results in the formation of a dry patch, which is responsible for the instantaneous jump in the wall temperature. When the bubble departs and moves away from the nucleation site, fresh liquid wets the surface and the wall temperature drops again. This is a classical flow instability and has a deadly influence on micro-channel heat exchanger.

When it comes to application on HCPVT system, the instability becomes more difficult to solve. The fundamental principle behind concentrating photovoltaics (CPV) is the substitution of expensive cell area with inexpensive optics [6]. As seen in Fig.3.1, parabolic dish concentrates sunlight on the heat exchanger by tracking the sun during the daytime, which means the heat exchanger is not fixed and also has to move with the concentrator. It brings a problem that heat exchanger is working at different orientation all the time, which might be the harshest working condition compared with heat sink working at stationary such as in data center or in the air-condition.

Fig.3.1: Scheme of the parabolic dish concentrator of HCPTV system

To figure out the orientation heat sink is working at, eq.3.1 is introduced to calculate the solar elevation angle,

$$\sin h = \sin\varphi \cdot \sin\delta + \cos\varphi \cdot \cos\delta \cdot \cos t \qquad (3-1)$$

$$\cos\alpha = \frac{\sin h \sin\varphi - \sin\delta}{\cos h \cdot \cos\varphi} \qquad (3-2)$$

$$\delta \cong 23.45 \cdot \sin(0.983540 \cdot n - 80.145404) \qquad (3-3)$$

$$t = 15 \cdot (T_t - 12) \qquad (3-4)$$

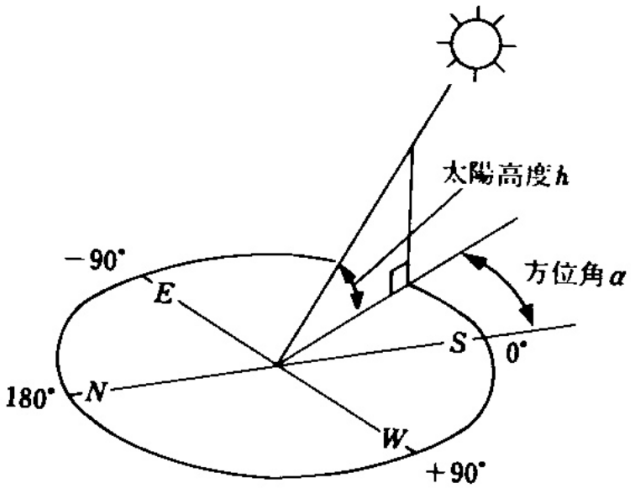

Fig.3.2: Sketch diagram of solar elevation angle

Where h is solar elevation angle, α is solar zenith angle, φ is latitude, δ is longitude, t is hour angel, n is represented the days from New Year's Day and T_t is solar time.

Thus, we found the heat exchanger working orientation in University of Tokyo, Kashiwa, Chiba, Japan (35.9N,139.94E) is at a range of 31.74 degrees to 78.26 degrees. In other words, the heat exchanger installed in HCPVT system is working almost vertically most of the time in winter. It makes flow boiling instability much more severe.

Bubble growth in the microchannel is the main cause of reverse flow instability of the two-phase flow. The fluid in the microchannel is governed by the surface tension, and when the fluid is continuously heated it evaporates and becomes bubbles. If the saturation liquid continues to be heated, the bubble expands rapidly. The pressure inside the bubbles increases and may become larger than the pressure of the inlet fluid, pushing the fluid back to the inlet and causing a reverse flow.

If reverse occurs in the channel, it would be fatal to the heat transfer performance because the downstream is being a lack of fluid and liquid film would evaporate quickly and never be replenished as long as the large pressure of vapor prohibits fluid coming into the channel. If downstream of microchannel could not be cooled, wall temperature would rise dramatically which is called dry-out flaw.

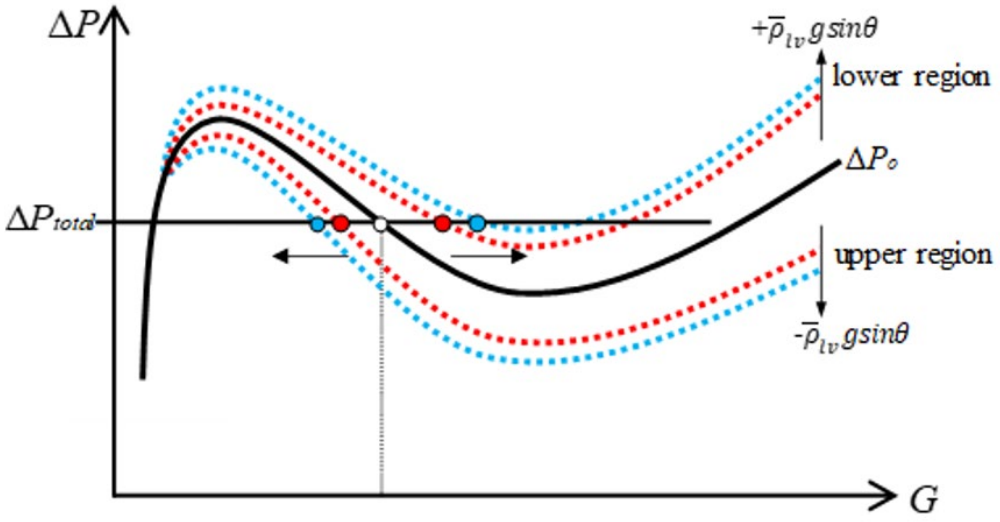

Fig.3.3: Relationship between pressure drop with mass flow during two-phase flow

From fig.3.3 is a curve calculated by Lockhart and Martinelli separated flow model, the pressure drop shows a N-curve with G when two-phase flow occurred. This curve is an evidence of flow maldistribution theoretically, cause of when the micro-channel working at vertical condition, the static pressure drop makes the gap between lower region and upper region larger, and the flow rate would be fluctuation between them.

What makes matters worse is, parabolic dish concentrator tracks the sun at a lower orientation about 11.74 degrees in winter as above, which means heat exchanger is working more like a perpendicular condition at that time. Fig.3.4 and fig.3.5 is a force analysis of a single channel, trying to account for how flow boiling instability occur and exploring the solution.

Compared two position of microchannel heat sink, as seen (a) and (b) in fig.3.3, when bubble is heated and inflates, in the upper part of HE buoyancy contributes to accelerate the vapor escape the channel, however, in the lower part of HE the buoyancy prevents bubble inflate and make vapor float upward to the inlet.

These two opposite phenomena in microchannel lead to significant discrepancy in the flow distribution among channel arrays. When placed non-horizontally, liquid starve may occur in the upper region, while the lower channels could be flooded with liquid but in lower vapor quality, which causes large temperature difference. When solar cell is installed on the surface of heat exchanger great gap of temperature would occur hot spots flaw or even burn-out of target solar cells. This flow maldistribution becomes more pronounced with the increase of orientation angle, hindering the application of two-phase flow heat sink.

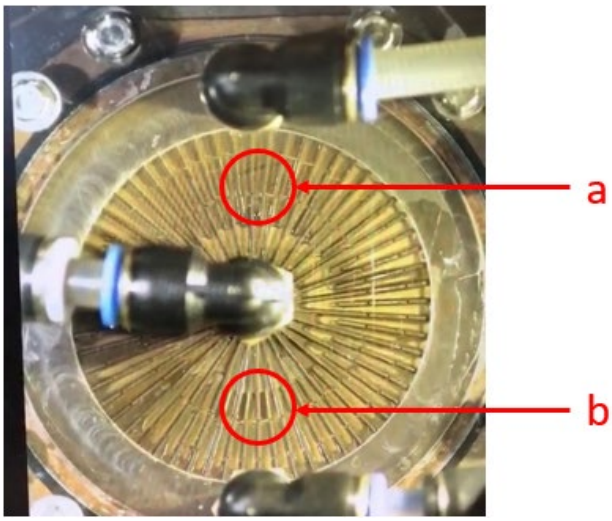

Fig.3.4: Choose two area to analysis

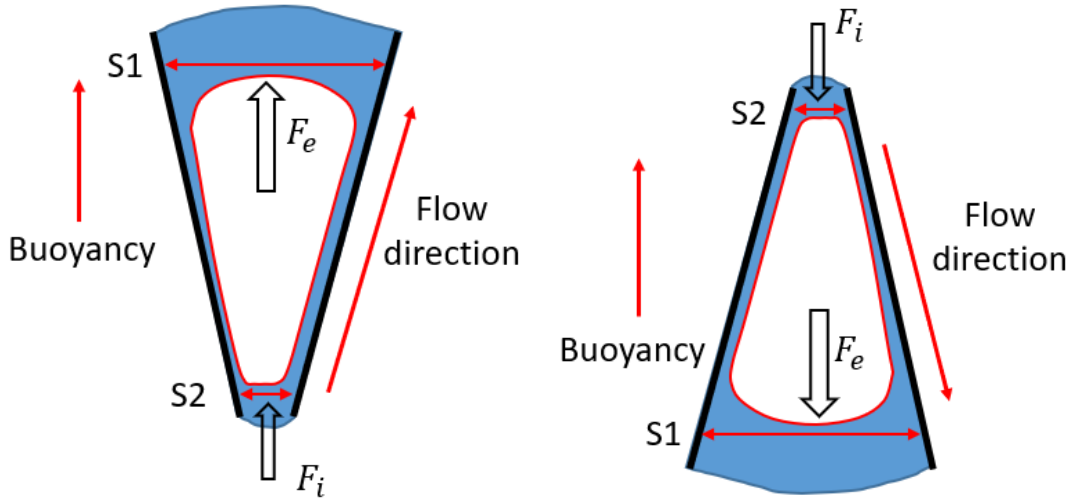

(a) In the upper part of HE (b) In the lower part of HE

Fig3.5: Sketch diagram of force analysis in a single micro-channel

Where F_i is represented inertia force, F_e is force of evaporation.

The misdistribution of flow in channel array is because the pressure in each channel is in a great difference. The flow increases where the pressure is small while dry-out occurs where the vapor prevents liquid coming. To account for it more specifically, the pressure drop in microchannel was calculated with Lockhart and Martinelli model. As seen in fig.3.6(a), pressure drop is a function of mass flow given by certain heat, even though the diameter of micro-channel is only 7cm, the large density of water makes the static pressure drop one-third of friction pressure drop in a single micro-channel. When in the vertical working condition, it is more pressure drop gap between upper and lower part of heat exchanger. Obviously, the effect of gravity on radial micro-channel cannot be neglected.

The influence of body force on fluid motion and therefore heat transfer in flow boiling systems is dictated by the magnitude of buoyancy force relative to other forces such as inertia and surface tension. Because of large density difference between phases, buoyancy can play a crucial rule in a flow boiling system. While very high coolant velocities are key to achieving this goal, such velocities greatly increase pressure drop and pumping power, resulting in adverse effects on thermodynamic efficiency of the cooling system.

To solve this cooling issue and ensure the solar cell working in a stable condition, although heat exchanger already meets the thermal performance, it needs to be improved in instability to conquer the influence of gravity.

A simple way to eliminate the effect of orientation is to increase the friction pressure drop in the micro-channel, for example, put a porous metal in front of each micro-channel to increase the friction pressure drop, calculated by Lockhart and Martinelli separated flow model, seen in fig.3.5 (b) if the friction pressure drop is increased 7000 Pa/m the proportion of static pressure drop would reduce from 35% to 20%. Thus, the pressure drop gap between the upper and lower of heat sink could be reduced which consequences the flow distribution more uniform and better in thermal characteristic.

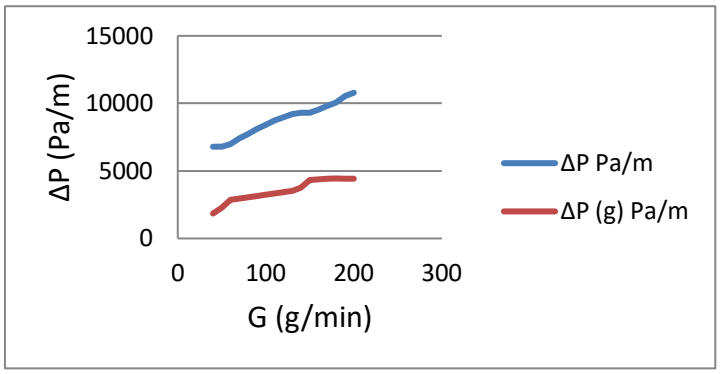

(a)

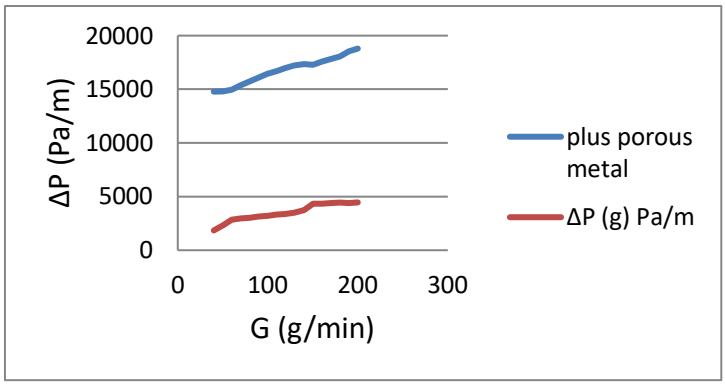

(b)

Fig.3.6: Pressure drop in micro-channel exchanger

3.2 Experiment of thermal characteristic with improved HE in different orientation

3.2.1 Experimental setup

An experimental loop is established to evaluate the effect of orientation on thermal performance of radial micro channel heat exchanger, the schematic diagram of which is shown

as Fig.3.7(a).

The main parts of setup are similar with the one in chapter 2. A micro gear pump (MICROPUMP GJ-DB380.A), a needle valve, a bypass loop and a flow meter (OVAL ALTI mass II CA001) were used to monitor and regulate the inlet mass flux. A thermostatic bath preheater was used to adjust the inlet subcooled degree of working fluid. A condenser was used to chill the outlet two-phase flow and stabilize the system outlet pressure. The different orientation angle was achieved by adjusting the upright height of test section, as shown in Fig.3.7 (b). The test section was as the same as previously introduced, which was made up of a polycarbonate cover plate, a copper base plate and a copper cartridge heater. An O-ring was used for sealing between cover plate and base plate. To detect the temperature distribution and temperature difference on HE, 4 thermocouples were symmetrically arranged from inlet to each outlet. All thermocouples were placed 5 mm below the surface of microchannel and inserted to the center cross-section of HE.

To calculate the saturation temperature of the system, it is necessary to measure the pressures at the outlet. Temperature and pressure at the inlet and outlet were both monitored, where K-type thermocouples and pressure sensor switch gauge (NAGANO KEIKI KP-15) were used. In the present work, the outlet pressure was controlled at 107.2±1 kPa, and the corresponding saturation temperature was maintained within 101.6±0.3 ^{o}C.

MEMRECAM high-speed digital camera (NAC Image Technology, HX-6), as shown in fig3.9, and two laser light sources were used to conduct visualization, where 500 frame/s (fps) and 1280 × 1280 dpi was set as the frame rate and spatial resolution, respectively. The placement of lens was confirmed for the visualization tests under different orientations.

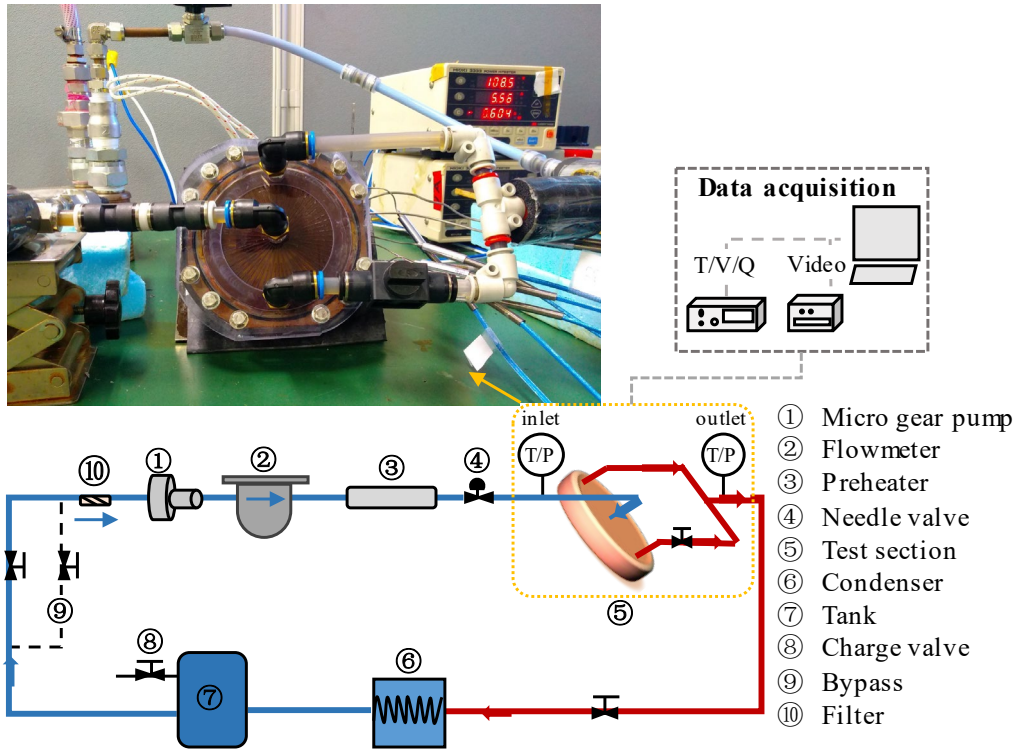

(a)Experimental loop

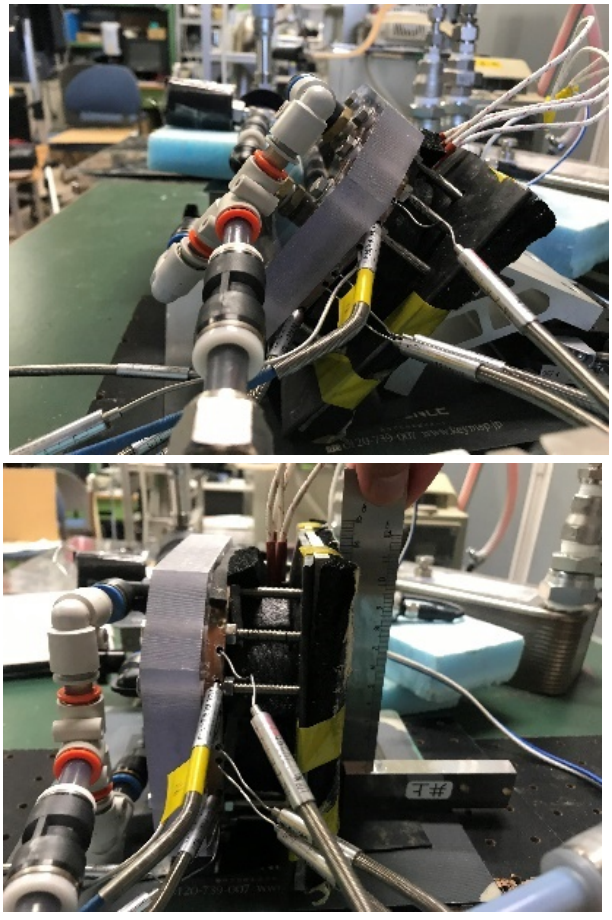

(b) Orientation setup

Fig.3.8: sketch and photo of experimental setup

Fig.3.9: High speed digital camera for visualization

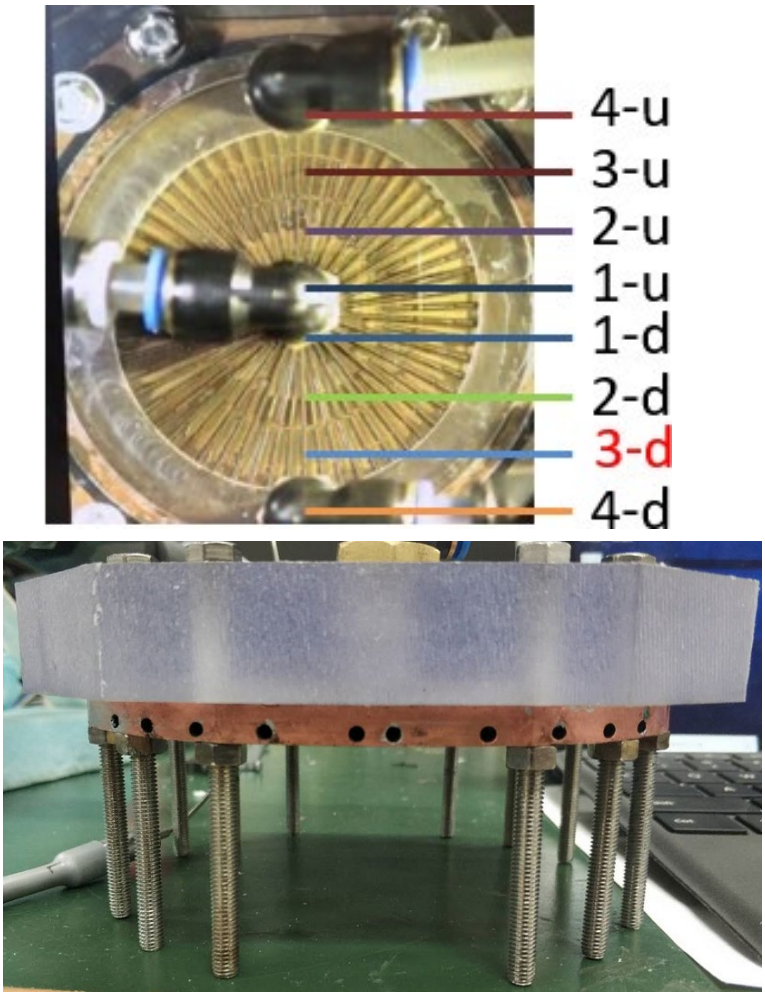

Fig.3.10: The measurement points of thermocouples

3.2.2 Test procedure and data processing

To examine the effect of orientation, flow boiling tests under five orientation angles including ∠ 0º, ∠ 60º and ∠ 90º have been investigated. Only the thermal performance, wall temperatures of heat exchanger, was processed because when applied in HCPVT system the most concerned is ensuring the solar cell in a stable and safe working condition. Thus, two main parameters were observed in testing, one is the wall temperature and the other is the temperature fluctuation. During the tests, if a sharp temperature rise occurred and T_{max}>120 ℃, cut off the power and terminated test. The testing condition is given as Table3.1,

Table.3.1: Test condition

Angle	G [kg/m^{2}s]	Q_{in} [W]	q_{eff} [kW/m^2]	T_{in} [ºC]
∠0º				84.3±0.3
∠60º	22.1	800	177.6	84.6±0.1
∠90º				84.1±0.3

To compare thermal performance, test section experimented with the same mass flow, heat flux and inlet temperature. Only changing the orientation during the test and keeps the other parameters the same. The heat flux of 17.6W/cm^2 is the highest can reached with current equipment. Theoretically, the vapor quality of each working condition would be same because the heat and mass flow are not changed. If the thermal performance changes, it should be the influence of gravity.

3.2.3 Result

The thermal performance of the proposed radial micro channel heat exchanger under various orientations is firstly examined under an extreme operating condition where low inlet mass flux and high heat flux are simultaneously applied. The results against orientations are displayed, as seen in fig.3.11 wall temperature as a function of time, with the orientation increasing from the horizontal (∠0º) to vertical (∠90º), the wall temperatures in the upper

region of HE oscillate more violently owing to the reduced mass flow and increased vapor quality, whereas the wall temperatures in the lower region barely oscillate but decrease slightly with the aid of the gravity.

That is to say, agree on the previous theoretical analysis on a single channel, in the upper region, the buoyancy contributes to being a positive factor to accelerate vapor escaping the channel, elevates the velocity of two phases of fluid. Thus, the convective heat transfer becomes better and wall temperature is lower than which placed in horizon. On the contrary, in the lower region of HE, after the bubble is getting bigger along the flow direction, the vapor stays stationary in the channel and even floats upper to the inlet of HE. As the same with theoretical derivation, the buoyancy presents a negative effect on thermal performance because the direction of buoyancy is against the inertia force of flow and makes the block of vapor be an obstacle in the channel, reducing the mass flow. As a kind of flow instability, the reverse flow occurs. The detail and comparison would be showed in visualization.

From the comparison of each orientation working conditions, even though violent temperature fluctuations are recorded with the increasing of orientation angle, T_{max} of wall temperature is maintained below 110℃ and ΔT_{max} is kept below 5 K, which meets the thermal management demand for PV-CSP system. Namely, the increasing of orientation angle brings about a certain temperature oscillation during the operation but an insignificant effect on the static thermal performance, proving that REMHS can operate satisfactorily for all orientations under the extreme condition. Besides, it is noted that the most violent temperature oscillation occurs at $\angle 60^{o}$ instead of $\angle 90^{o}$, which illustrates that the variation of thermal performance against orientation is non-linear, which is also consist with the recorded high-speed visualization results.

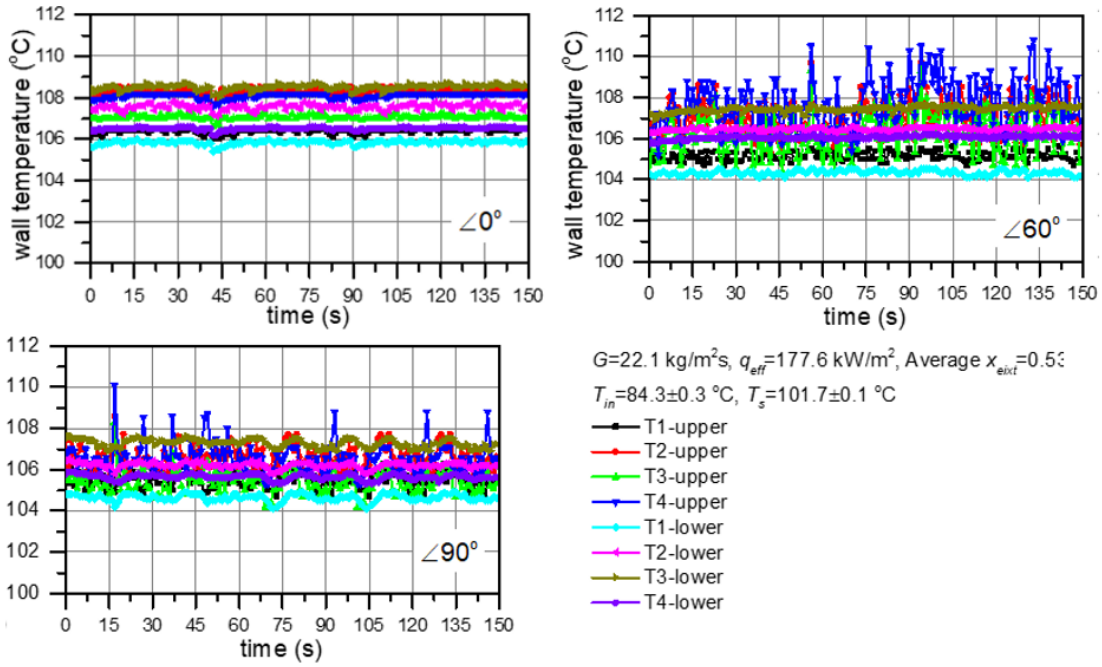

Fig.3.11: Dynamic variations of wall temperature

3.3 Visualization

Fig. 12 compares the visualization results of dynamic two-phase flow in radial micro-channel heat exchanger under ∠0°, and ∠90° in a same time interval. It is confirmed that the temperature oscillation in the upper region of HE is resulted from intermittent vapor choke and relief in the upper channels under reduced mass flow and increased vapor quality. As expected, the expand cross-section area of microchannel facilitates the elongated vapor plugs to move spontaneously towards the outlet instead of complete blocking the channel.

When heat sink working at horizon, as seen in visualization of ∠0°, the flow distribution was almost uniform in each micro-channel, both upper and lower region of heat sink were filled with fluid. Bubbles were growing up along with the flow direction and escaping successfully. No reverse flow was observed during the test. When it comes to thermal performance, the results of visualization are in accord with fig.3.11 which the wall temperature is stable.

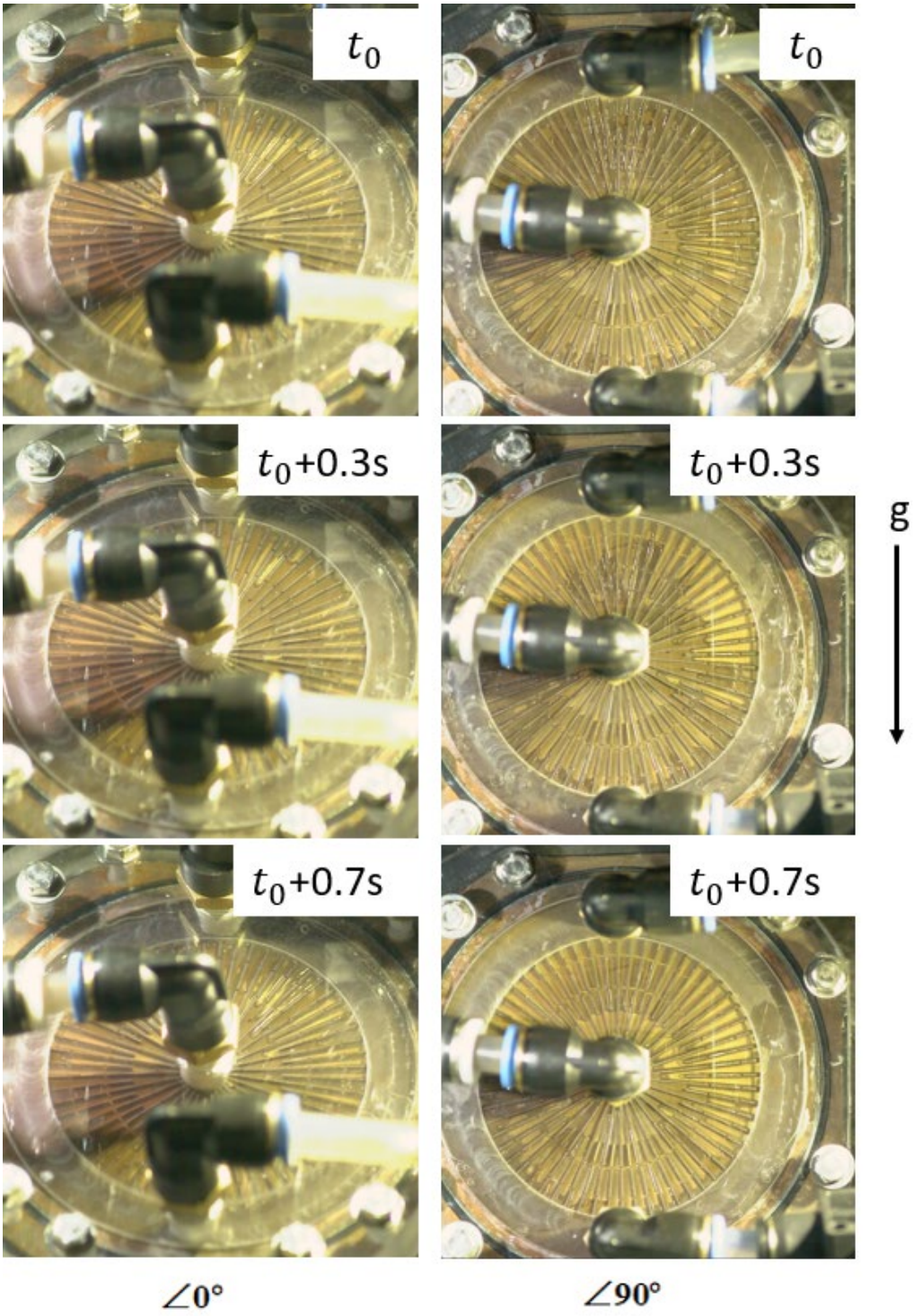

Fig.3.12: Visualization result of intermittent vapor blockage in HE under various orientations

However, as seen in the visualization of ∠90°, when HE working at vertical condition, vapor was almost aggregating at the upper of HE and prevented fluid flowing into the channel. As a result, the upper region of microchannel was filled with high vapor quality two-phase flow

and it was evaporated in a short time. Thus, dry-out was observed in upper region which is keeping with fig.3.11 that temperature oscillation occurred. On the contrary, the lower region of HE was filled with very low vapor quality two-phase flow. All of these phenomena could be accounted for the effect of gravity on micro-channel heat transfer.

3.4 Experiment of the thermal characteristic with improved radial expansion microchannel heat exchanger

After theoretical analysis and experiment on the effect of gravity on the heat exchanger, it is clear that gravity has a tremendous influence on micro-channel heat exchanger, so a solution was introduced to solve this problem.

According to the similar solution in parallel array micro-channel heat exchanger, as seen in fig.3.13: an inlet restrain structure was set behind the each of micro-channel aims to increase the friction pressure drop. A porous metal was set in front of each micro-channel in order to elevate the total pressure drop to suppress the effect of static pressure drop in micro-channel heat exchanger.

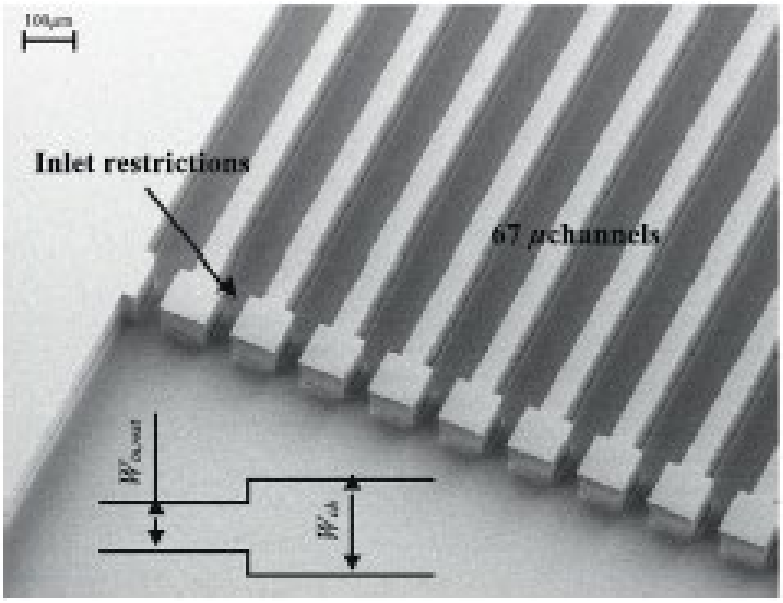

Fig.3.13: Inlet restriction

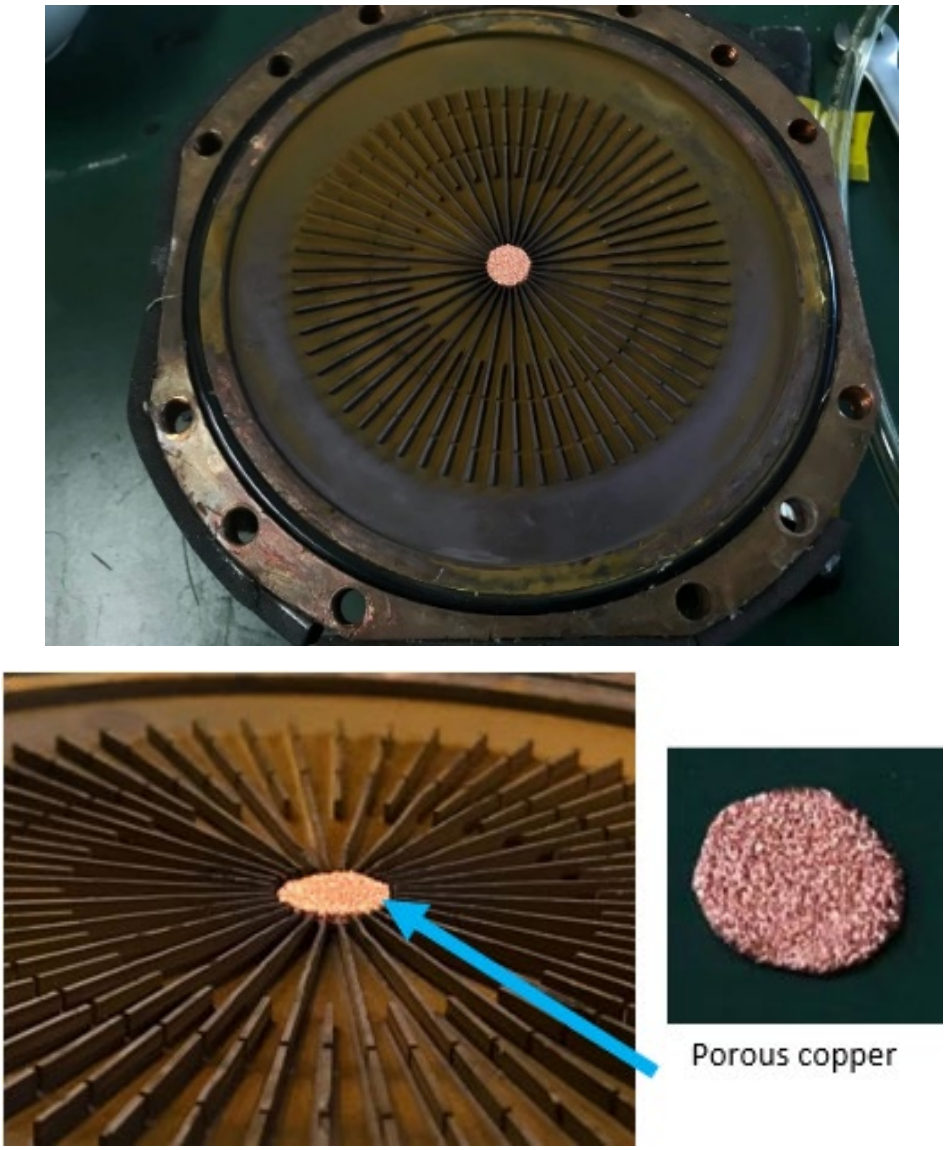

Fig.3.14: Porous copper placed in front of each channel

As seen in fig.3.14, a circular porous copper was placed at the center of heat sink where is the initiation of each micro-channel. Fluid vertically flows to the heat sink and passes throughout the porous copper firstly.

The experiment setup is the same as the loop as above, the only difference is planting a porous copper. The testing condition is shown in table.3.2,

Table.3.2: Testing condition of heat sink

Angle	G [kg/m^{2}s]	Q_{in} [W]	q_{eff} [kW/m^2]	T_{in} [ºC]
∠90º	71	800	177.6	80.1±0.3

As the thermal performance is the worst in vertical condition, only $\angle 90^{o}$ is tested during experiment. As seen in fig.3.15, which is the temperature distribution on the surface of heat exchanger, after planting the porous copper in front of the micro-channel, the temperature oscillation was eliminated and also kept a good heat transfer characteristic as before. That is to say, planting porous copper to elevate total pressure drop could relieve the effect of gravity on micro-channel heat sink with a diameter of 8cm.

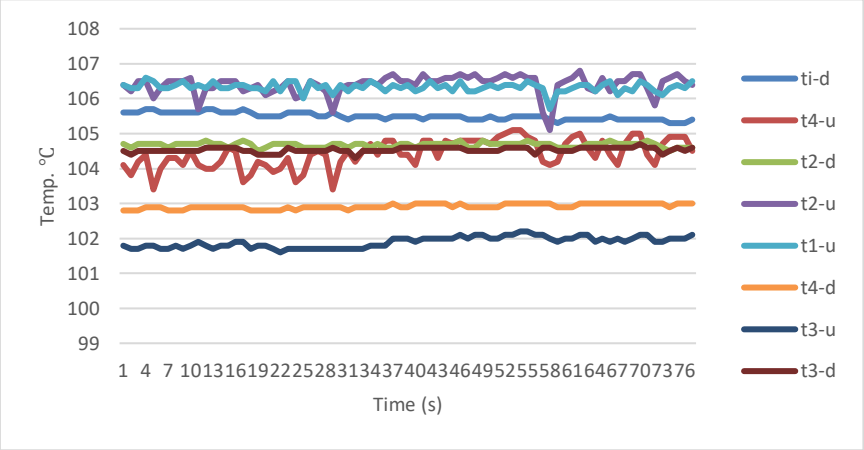

Fig.3.15: Thermal characteristic of improved heat sink at vertical and the position of thermocouples

Chapter 4 Experiment of thermal performance on HCPVT system with improved microchannel heat exchanger

In high concentrating photovoltaic (HCPV) systems the sunlight is collected by concentrating optics and focused onto a considerably smaller photovoltaic receiver. Thus, this technology substitutes expensive photovoltaic cell material by inexpensive optical equipment. This approach reduces the cost per produced kilowatt-hour [4,5].

All solar concentrator systems share some key requirements. Thermal management and temperature control are among the most important aspects in any concentrator system because of the generated high-power densities. Especially CPV systems require strict temperature control because of the strong influence of the operation temperature on the photovoltaic conversion process. The electrical efficiency and, consequently, the power output of a photovoltaic module depend linearly on the operating temperature [13].

All over the work introduced in this article serves for an ultimate goal that is to realize the co-generation of HCPVT system. From the point view of heat transfer, ultimate is to carry out the thermal control of solar cell while concentrated with a huge heat flux. After solving the heat transfer performance and the effect of gravity, it is time to apply radial micro-channel heat exchanger on the parabolic concentrator and investigate the overall performance of HCPVT system.

Fig.4.1: Concentrator and receiver of HCPVT system

4.1. Experiment setup

The experimental setup is similar with the loop in Chapter 2&3, the schematic diagram of experimental loop is shown as Fig.4.2(a). Deionized water was used as the working fluid. The inlet liquid was supplied by a micro gear pump (MICROPUMP GJ-DB380.A), and the flowrate was measured by a mass flow meter (OVAL ALTI mass II CA001) before flowing into test section. The temperature of inlet subcooled liquid was regulated at a range of 70 ℃ to 80℃ by a thermostatic bath preheater because after discussed in Chapter 2, the flow boiling heat transfer coefficient is little correlation with subcooled temperature and also the preheater bath is a simple one which made by myself, it is hard for it to sustain a high and permanent inlet temperature. The two-phase flow outflowed the test section was cooled down by a condenser before the tank otherwise the outlet pressure drop would be greatly unstable, it leads to a variation in flow rate.

The sunlight reflected by parabolic concentrator is the source of heat, which could be calculate by direct solar radiation and reflectance of concentrator. The direct solar radiation is measured by a radiometer, shown in fig.4.3.

The test section was tracking the sun along with the concentrator and installed 3cm away from the focal of the concentrator to relieve the heat flux below the CHF of heat sink because the concentration ratio at the focal would be 3000 $xsuns$ (times of solar radiation) which is an extremely huge of heat flux could not been cooled yet in the world.

The test section and all connecting pipes were wrapped with thick asbestos fabric for thermal insulation. The temperatures at the inlet and outlet were measured by K-type thermocouples. The pressures at the inlet and outlet were measured by pressure sensor switch gauge (NAGANO KEIKI KP-15), the outlet pressure was maintained at 107.2 ± 1 kPa by the test bench, and the corresponding saturation temperature was within 101.5 ± 0.5 _C. The inlet/outlet pressure were recorded in a frequency of 500 ls with a high-speed analog measurement unit (NR-HA08).

The schematic diagram of test section and thermocouple locations are displayed as Fig.4.2. HE consists of a copper base plate (7 mm in height), and a polycarbonate cover plate (30 mm in height) for the convenience of visualization. An O-ring was used for sealing.

Shown as Fig.4.4, 3 test points were symmetrically arranged in HE to detect the distribution

of wall temperature along the radial direction. The thermocouples were 5 mm beneath the bottom surface of channel.

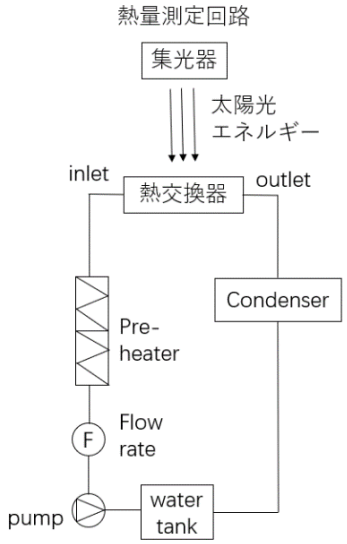

(a) Sketch diagram of experiment loop

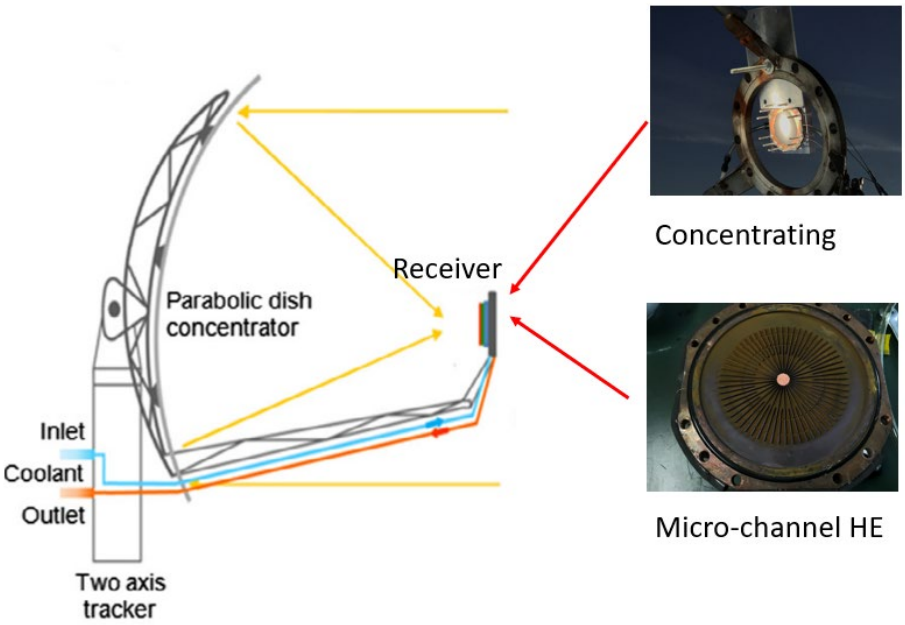

Fig.4.2: Sketch of HCPVT system and receiver

Fig.4.3: EKO MS-57 direct radiometer

4.2. Thermal characteristics

Thermal performance was experimented by loop as above, apart from three temperature measurement points beneath the surface of micro channel heat exchanger, the parameters of inlet temperature, outlet temperature, direct solar radiation and total solar radiation were conducted in the test. The working condition is introduced as table.4.1,

Table 4.1: Working condition of heat sink

G [g/min]	q_{eff} [W/cm^2]	T_{in} [ºC]	T_{sat} [ºC]	*Angle* [º]	*Concentration ratio*	*Radiation* [W/ m^2]
163	82.4	69	102.2	64	1070*xsuns*	770

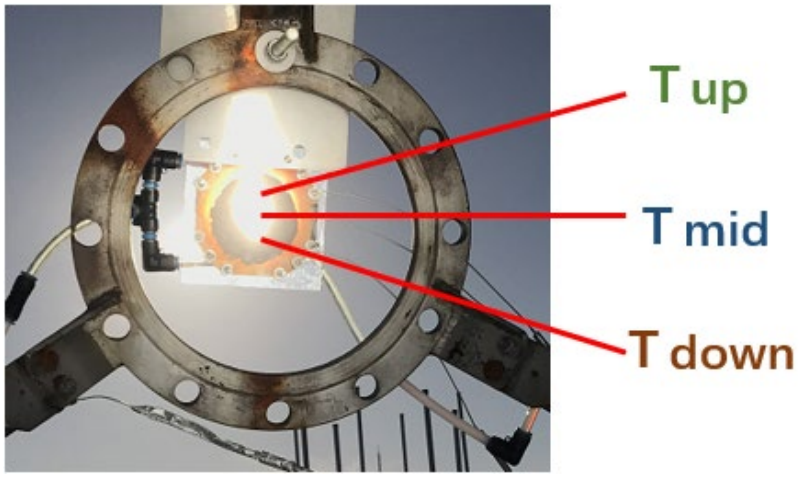

Fig.4.4: Three temperature measurement points by thermocouples

As shown in fig4.5 (a), the out let curve is almost unchanged about 102 ºC which means the

radial micro-channel heat sink is working in a stable two-phase flow heat transfer condition, also the solar radiation is stay unchanged with time which means the heat flux concentrated on heat sink is a certain value. It brings a stable condition to evaluate the thermal performance of heat sink.

Fig.4.5 (b) is the wall temperature and solar radiation as a function of time, for an average of temperature, $T_{up} = 105.7℃$, $T_{mid} = 105.2℃$, $T_{down} = 104.3℃$. The difference between T_{up} and T_{down} is only 1.4℃, it means the temperature distribution of surface is uniform. In other words, the flow instability caused by gravity was relieved successfully. More importantly, the maximum of surface temperature is only 106.7℃ under the heat flux of 82.4W/cm^2, concentration ratio of 1060 $xsuns$.

The temperature difference of T_{up} with T_{sat} would be 3.5℃. That is to say, the heat transfer coefficient would be as high as 235,428W/m^2K. For 3-junction solar cell which usually could work below 150℃, the heat transfer performance is capable to sustain it in HCPVT system. Although in particle, the thermal resistance of solar cell and solder or silicon grease is evitable to create a temperature elevation during concentrated, the thermal characteristics of heat sink successfully meet the requirement of cool the solar cell.

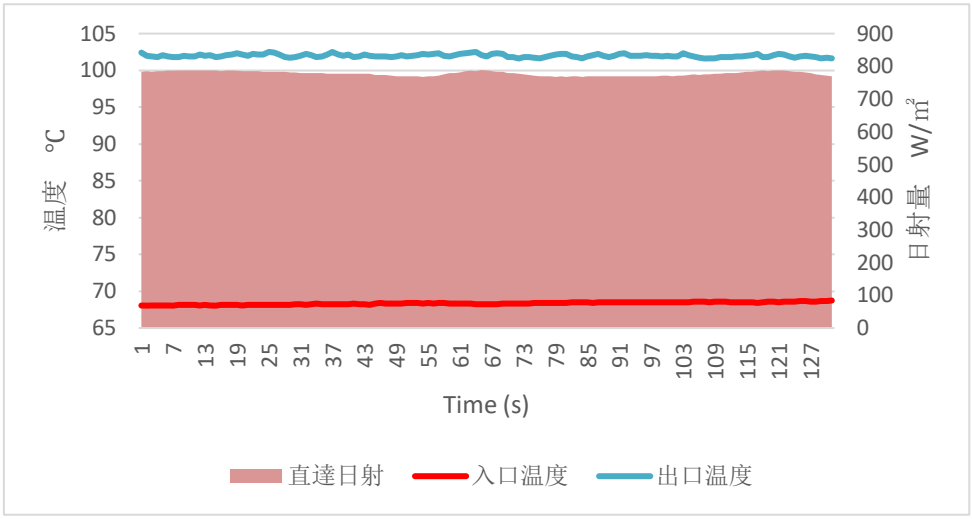

(a) Distribution of solar radiation and inlet/outlet condition

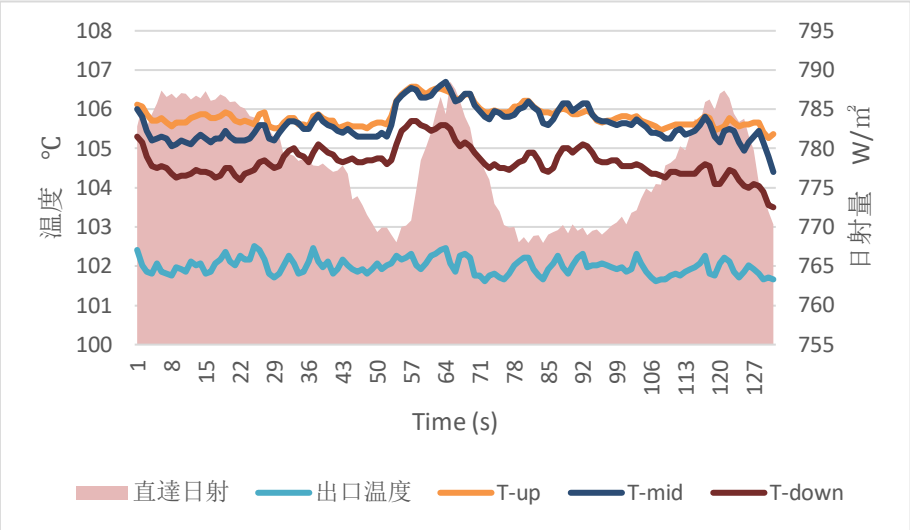

(b) Distribution of Surface temperature and direct solar radiaiton

Fig.4.5: Thermal characteristics of radial micro-channel heat sink in HCPVT sytem

Chapter 5 Conclusion

A new-type radial expanding micro-channel heat exchanger was designed and when apply it in the parabolic dish concentrator, the maximum of surface temperature is only 106.7℃ under the heat flux of 82.4W/cm^2, concentration ratio of 1060 $xsuns$.

Moreover, the flow instability caused by gravity was suppressed successfully by theory and experiment. It ensures the heat sink maintaining a high thermal performance in various orientations.

When concentrating, the heat transfer coefficient would be as high as 235,428W/m^2K. For 3-junction solar cell which usually could work below 150℃, the heat transfer performance is capable to sustain it in HCPVT system. Although in particle, the thermal resistance of solar cell and solder or silicon grease is evitable to create a temperature elevation during concentrating, the thermal characteristics of heat sink successfully meet the requirement of cool the solar cell.

References

1) C. Wolfram, O. Shelef, P. Gertler, How will energy demand develop in the developing world, J Econ. Persp. 26 (1) (2012) 119–138.
2) Primary energy, Statistical Review of World Energy 2012, 2012.
3) M.A. Green, K. Emery, Y. Hishikawa, W. Warta, E.D. Dunlop, Solar cell efficiency tables (version 42), Progr. Photovoltaics 21 (5) (2013) 827–837.
4) D. Faiman, S. Biryukov, K.K. Pearlmutter, PETAL: a research pathway to fossilcompetitive solar electricity, I. IEEE, 2002.
5) Xudong Zhao, Xiaoli Ma," Advanced Energy Efficiency Technologies for Solar Heating, Cooling and Power Generation", pp. 32-35, 2019
6) Wolf M. Performance analyses of combined heating and photovoltaic power systems for residences. Energy Convers 1976;16(1):79–90.
7) Gang P et al. Annual analysis of heat pipe PV/T systems for domestic hot water and electricity production. Energy Convers Manage 2012;56:8–21.
8) Rabl A. Comparison of solar concentrators. Sol Energy 1976;18(2):93–111.
9) Kurtz S, Geisz J. Multijunction solar cells for conversion of concentrated sunlight to electricity. Opt Express 2010;18(101):A73–8.
10) Meneses-Rodrı´ guez D et al. Photovoltaic solar cells performance at elevated temperatures. Sol Energy 2005;78(2):243–50.
11) Brogren M, Nostell P, Karlsson B. Optical efficiency of a PV-thermal hybrid CPC module for high latitudes. Sol Energy 2001;69:173–85.
12) Luque A et al. Some results of the EUCLIDES photovoltaic concentrator prototype. Prog Photovoltaics: Res Appl 1997;5(3):195–212.
13) Chen H et al. Thermal analysis of a high concentration photovoltaic/thermal system. Sol Energy 2014;107:372–9.
14) Rosell J et al. Design and simulation of a low concentrating photovoltaic/ thermal system. Energy Convers Manage 2005;46(18):3034–46.
15) Chengdong K, Zilin X, Qiang Y. Outdoor performance of a low-concentrated photovoltaic-thermal hybrid system with crystalline silicon solar cells. Appl Energy 2013;112:618–25.

16) S.-W. Kang, Y.T. Chen, G.-S. Chang, The manufacturing and test of (1 1 0) orientated silicon based micro heat exchanger, Tamkang J. Sci. Eng. 5 (3) (2002) 129–136.

17) M.M. Mahmoud, T.G. Karayiannis, D.B.R. Kenning, in: Emerging Topics in Heat Transfer Enhancement and Heat Exchangers, WIT Press, 2014, pp. 321–396 (Chapter 10).

18) Y. Taitel, Flow pattern transition in two phase flow, Keynote lecture, in: 9th International Heat Transfer Conference, Jerusalem, Israel, 19–24 August 1990, pp. 237–254.

19) D. Barnea, An unified model for predicting flow-pattern transitions for the whole range of pipe inclinations, Int. J. Multiphase Flow 13 (1) (1987) 1–12.

20) J. R. Thome, “Boiling in microchannels: A review of experiment and theory,” Int. J. Heat Fluid Flow, vol. 25, no. 2, pp. 128–139, 2004.

21) 辰洋植田, 気液二相流-流れと熱伝達-. 養賢堂, 1981.

22) L. R.W. and M. R.C., “Proposed correlation of data for isothermal two-phase, two-component flow in pipes.” Chem. Eng. Prog. 45, pp. 39–48, 1949.

23) G. Wang, P. Cheng, H. Wu, Unstable and stable flow boiling in parallel microchannels and in a single microchannel, Int. J. Heat Mass Transfer 50 (21–22) (2007) 4297–4310.

24) X. Fu, S.L. Qi, P. Zhang, R.Z. Wang, Visualization of flow boiling of liquid nitrogen in a vertical mini-tube, Int. J. Multiphase Flow 34 (4) (2008) 333– 351.

25) M.R. Aligoodarz, Y. Yan, D.B.R. Kenning, Wall temperature and pressure variations during flow boiling in narrow channels, Proc.11th Int. Heat Transfer Conference (IHTC), August 23–28, vol. 2, 1998, pp. 225–230.

26) S.L. Qi, P. Zhang, R.Z. Wang, L.X. Xu, Flow boiling of liquid nitrogen in microtubes: Part I – the onset of nucleate boiling, two-phase flow instability and two-phase flow pressure drop, Int. J. Heat Mass Transfer 50 (25–26) (2007) 4999–5016.

27) S.G. Kandlikar, Nucleation characteristics and stability considerations during flow boiling in microchannels, Exp. Therm. Fluid Sci. 30 (2006) 441–447.

28) E.M. Fayyadh, M.M. Mahmoud, T.G. Karayiannis, Flow boiling heat transfer of R134a in multi microchannels, Int. J. Heat Mass Transfer (2016) (Submitted for publication).

29) J.C. Chen, A correlation for boiling heat transfer to saturated fluid in convective flow, ASME Paper, 63-HT-34 (1963) 1–11.

30) M.M. Shah, A new correlation for heat transfer during flow boiling through pipes,

ASHRAE Trans. 82 (2) (1976) 66–86.

31) S.S. Kutateladze, Fundamentals of Heat Transfer, Edward Arnold, London, 1963.

32) 中村亘 and 飛原英治, “2014 年度卒業論文 太陽光・太陽熱の同時活用システムの研究,” 2014.

33) 飛原英治, 原上青, and 党超鋲, “三接合太陽電池を用いる集光型ソーラーコジェネレションシステムに関する研究,” 太陽/風力エネルギー講演論文集, 2016.

34) 鄭晨 and 飛原英治, “修士論文 高熱流束マイクロチャンネル冷却器の研究,” 2017.

35) 濵田未勇 and 飛原英治, “修士論文 高倍率集光型太陽エネルギーの利用 に関する研究,” 2018.

36) S.G. Kandlikar, Review and projections of integrated cooling systems for threedimensional integrated circuits, Trans. ASME, J. Electronic Packag. 136 (024001) (2014) 1–11.

37) T.V. Oevelen, J.A. Weibel, S.V. Garimella, The effect of lateral thermal coupling between parallel microchannels on two-phase flow distribution, Int. J. Heat Mass Transf. 124 (2018) 769–781.

38) Y.W. Kuang, W. Wang, J.Y. Miao, X.G. Yu, H.X. Zhang, R. Zhuan, Flow boiling of ammonia and flow instabilities in mini-channels, Appl. Therm. Eng. 113 (2017) 831–842.

39) T.G. Karayiannis, M.M. Mahmoud, Flow boiling in microchannels: Fundamentals and applications, Appl. Therm. Eng. 115 (2017) 1372–1397.

40) S.G. Kandlikar, Nucleation characteristics and stability considerations during flow boiling in microchannels, Exp. Therm. Fluid Sci. 30 (5) (2006) 441–447.

41) S.H. Kim, I.C. Chu, M.H. Choi, D.J. Euh, Mechanism study of departure of nucleate boiling on forced convective channel flow boiling, Int. J. Heat Mass Transf. 126 (2018) 1049–1058.

42) S. Hong et al, Experimental investigation on flow boiling in radial expanding minichannel heat sinks applied for low flow inertia condition, International Journal of Heat and Mass Transfer 143 (2019) 118588

Acknowledgment

When I consulted senior students' thesis for reference, the part that I most interested in is the acknowledgment. From this part, I can see people writing something from his own heart, never need to disguise anymore because nobody is concerned with the acknowledgment in a thesis. Unfortunately, I did.

So, I found the senior students were not only a distinguished researcher but also an affectionate people, they were all truly appreciate to advisor and the University of Tokyo. Of course, me too.

Actually, I have nothing but appreciation to my advisor professor Dang. He gave me a chance to have access to the top research laboratory in the world. And during my master's studying, professor Dang was always teaching me how to solve technical problem with knowledge, more important is he taught me how to be a better people. Thanks professor Dang picked me up and gave me such a great chance to do research and study in such fantastic environment, whenever I get frustrated in doing research, the motivation to support me was to repay the advisor's trust.

Obviously, I am not a talented person in doing research, but I am willing to spend time and no fear to face failure. Professor Hihara is the chief of our group, he is full of wisdom and kindness all the time and always encourages me in doing experiment. What impresses me most is such an outstanding scholar like Hihara always did cleaning for our laboratory. I felt ashamed of myself, professor Hihara taught me that to be a people with good manner is as important as study. Undoubtedly, it is a great honor for me to study in such an excellent laboratory and learn from professor Hihara and professor Dang.

During my study time in University of Tokyo, all members of our group gave me power and much help in doing research. Hong sihui, Cao xufa, Xu jingren, Cheng zhizhong, Song mengjie, Zhang zhihua, Hirai shyo and so many members I would like to appreciate. Distinctly, without the help of them, it is no way for me to graduate. Thanks for the accompanying in the study and daily life.

Last but not least, I would like to write something for my parents and my girlfriend. There is a little space for acknowledgment but the length could not show my love. They all the treasure for me, it is true I made you mad and had countless quarrels during daily life, but you stood up when I overwhelmed with fear and terror, that is enough.